**MASTER EN SCIENCES PHYSIQUES À FINALITÉ SPÉCIALISÉE EN PHYSIQUE DU VIVANT**

# Application of TOF-SIMS for the detection of proteins using antibodies conjugated to metal nanoparticles

WATTIEZ, Abigail

*Award date:*
2023

*Awarding institution:*
Universite de Namur

University of Namur

Sciences Faculty

# APPLICATION OF TOF-SIMS TO THE STUDY OF PROTEINS LABELED BY ANTIBODIES CONJUGATED TO METALLIC NANOPARTICLES

**Master's thesis presented for the award of the academic degree of Master in Physical Sciences - Specialized field (Physics of living organisms)**

Abigail WATTIEZ

June 2023

## Acknowledgments

I would like to express my heartfelt gratitude to every person who has supported me during the past two years of my master's program and has contributed to the completion of this work. First and foremost, I am deeply thankful to my supervisor, Professor Laurent Houssiau, for placing his trust in me during my master's thesis and for providing invaluable support and guidance.

I had the privilege of collaborating with numerous individuals from various laboratories, and I would like to extend my special thanks to the researchers from the LARN, particularly Sebastien Penninckx and Anne-Catherine Heuskin, for their unwavering availability and kindness in addressing all of my questions. I am also grateful to everyone who has contributed to expanding my knowledge and fostering my interest in the diverse techniques employed in their respective laboratories.

The contributions of LabCeTi have been crucial in the accomplishment of this work. They have not only addressed all of our doubts but have also facilitated numerous reflections and discussions. I am sincerely grateful for the opportunity to learn a wide range of biological techniques, thanks to their support. I would also like to express my gratitude to URBC and URBV for their significant contributions to my scientific development.

I was fortunate to have a supportive environment in LISE. Without the assistance of Alexandre Felten, I would not have been able to learn the complexities of using ToF-SIMS independently. Alexandre was always available to help with any problems or questions that arose. Moreover, I am grateful to the individuals at LISE and LPS who warmly welcomed me and with whom I shared amazing lunchtimes, filled with laughter and meaningful discussions about the results of my master's thesis. Their suggestions were consistently valuable. I consider myself fortunate to be surrounded by such caring individuals on a daily basis.

No acknowledgment section would be complete without mentioning Xavier Delvaux, who has been involved in every aspect mentioned above. Xavier's unwavering trust and constant support have been invaluable. Working with him has been a remarkable experience, as he is not only a highly skilled professional but also a patient, supportive, and humorous person. Xavier has taught me more than I could have ever learned in the past five years. In addition to his scientific guidance, he has been a pillar of moral support, always ready to uplift me during moments of doubts.

Lastly, I would like to extend a special thank you to my family, friends, and partner for their unwavering support and care throughout my studies. I am deeply grateful for the love and trust they have shown me.

Enseignement du Département de Physique
Rue de Bruxelles 61 - 5000 NAMUR
Téléphone: + 32(0)81.72.44.90 - Téléfax: + 32(0)81.72.44.64
E-mail: enseignement.physique@unamur.be - http://www.unamur.be

# APPLICATION DU TOF-SIMS À L'ÉTUDE DE PROTÉINES MARQUÉES PAR ANTICORPS CONJUGUÉS À DES NANOPARTICULES MÉTALLIQUES

WATTIEZ Abigail

## Résumé

Le ToF-SIMS (Time-of-Flight Secondary Ion Mass Spectroscopy) est une technique de spectrométrie de masse vastement utilisée en physique des matériaux, utilisant un faisceau d'ions pour bombarder des échantillons et en extraire des fragments caractéristiques. Récemment, il lui a été découvert un grand potentiel pour l'analyse de systèmes biologiques complexes, dans lesquels notamment la distribution de molécules organiques peut être obtenue. Cependant, l'étude de protéines, pourtant très importante en biologie, est difficile en ToF-SIMS, car il permet d'obtenir des informations caractéristiques uniquement pour des molécules d'environ 2000 uma maximum, ce qui limite son utilisation.

Cette étude vise à lever cette limitation et contribuer au développement d'une méthode de marquage spécifique de protéines dans des systèmes biologiques complexes, tels que l'épiderme humain, et leur cartographie en ToF-SIMS, via des anticorps conjugués à des nanoparticules métalliques. Ces dernières donnant un signal connu en ToF-SIMS, la distribution spatiale donne la distribution des protéines marquées par nanoparticule. Ce travail porte sur la caractérisation des nanoparticules, suivie de leur bioconjugaison à des anticorps grâce à une molécule de couplage, et sur la caractérisation du bioconjugat formé. Le marquage sur des épidermes reconstruits a dû être optimisé et a été réalisé sous différentes conditions et différentes analyses ToF-SIMS.

Les résultats ont montré que la bioconjugaison était effective et que le marquage avait permis de cibler une protéine d'intérêt dans un épiderme reconstruit. Les expériences qui ont été réalisés ont permis de déterminer les conditions optimales du marquage et ont servi de solide base pour la réalisation d'un marquage totalement spécifique et précis.

*Mots clés* : ToF-SIMS, nanoparticules d'or, marquage indirect, bioconjugaison, protéines.

Mémoire en Sciences Physiques - Finalité Spécialisée

Juin 2023
**Promoteur** : Laurent Houssiau
**Encadrant** :Xavier Delvaux

Enseignement du Département de Physique
Rue de Bruxelles 61 - 5000 NAMUR
Téléphone: + 32(0)81.72.44.90 - Téléfax: + 32(0)81.72.44.64
E-mail: enseignement.physique@unamur.be - http://www.unamur.be

# APPLICATION OF TOF-SIMS TO THE STUDY OF PROTEINS LABELED BY ANTIBODIES CONJUGATED TO METALLIC NANOPARTICLES

WATTIEZ Abigail

## Abstract

Time-of-Flight Secondary Ion Mass Spectroscopy (ToF-SIMS) is a widely used mass spectrometry technique in materials sceinces, which uses an ion beam to bombard samples and extract characteristic molecular fragments. Recently, it has been discovered that ToF-SIMS has great potential for the analysis of complex biological systems, in which the distribution of organic molecules can be obtained. However, the study of proteins, which are very important in biology, is challenging in TOF-SIMS because it only allows obtaining characteristic information for molecules of around 2000 amu maximum, which limits its use.

This study aims to overcome this limitation and contribute to the development of a specific labelling method for proteins in complex biological systems, such as the human epidermis and their mapping in ToF-SIMS, via antibodies conjugated to metallic nanoparticles. These provide a known signal in TOF-SIMS and the spatial distribution gives the distribution of proteins labelled by nanoparticles. This work focuses on the characterization of nanoparticles, followed by their bioconjugation to antibodies using a coupling molecule and on the characterization of the formed bioconjugate. The labelling on reconstructed epidermis had to be optimized and was performed under different conditions and TOF-SIMS analyses.

The results showed that bioconjugation was effective and that the labelling had targeted a protein of interest in reconstructed epidermis. The experiments carried out enabled us to determine the optimum conditions for marking and provided a solid basis for the creation of a totally specific and precise marker.

*Keywords* : ToF-SIMS, gold nanoparticles, indirect labelling, bioconjugation, proteins.

Master's thesis in Physics – Specialised finality

June 2023
**Promoter** : Laurent Houssiau
**Supervisor** :Xavier Delvaux

# Table of contents

# 1. Introduction

The technique known as ToF-SIMS, short for "Time-Of-Flight Secondary Ion Mass Spectrometry", is a widely used mass spectrometry technique in materials sciences that operates under ultra-high vacuum conditions [1]. It shows excellent surface sensitivity in the order of the ppm and allows for depth profiling analysis under certain conditions, as well as the mapping of elements of interest. The principle is based on a surface sputtering mechanism using a beam of monoatomic or polyatomic ions. A fraction of the ejected atomic and molecular species is ionised and accelerated towards a detector, allowing to reconstruct mass spectra as well as images of the samples.

ToF-SIMS is of great interest in the field of surface analysis, providing valuable information about the chemical composition of surfaces, as well as the presence of impurities [1]. This technique has many applications, ranging from the characterization of polymers, semiconductors and metals to the detection of organic contaminants [2]. More recently, ToF-SIMS has been used in biology where it has proved successful in identifying lipids [3], elucidating the mechanisms behind drug diffusion and contributing to studies of bone regeneration [4].

Despite its usefulness, ToF-SIMS has a limitation in detecting molecules larger than 2000 atomic mass units (amu). While this limitation does not affect the detection of lipids, it poses a significant challenge in analysing larger molecules such as proteins, macromolecules that can have a mass of several hundred thousand kDa. Fragments of 2000 amu are thus far from being comparable to the size of what could be considered a characteristic fragment of a protein. This work aims to overcome this by developing a specific labelling technique of proteins in a complex system. Reconstructed human epidermis being a current research topic in the laboratory, these were chosen.

To overcome this limitation, it has been proposed to carry out a labelling with metallic nanoparticles (NP) in order to indirectly follow the distribution of a protein of interest in a reconstructed epidermis. If we succeed in labelling the protein of interest with an antibody conjugated to a metallic nanoparticle, it is hoped that ToF-SIMS analysis will allow to observe the signal from the metallic nanoparticle and distinguish it from the organic component of the signal. ToF-SIMS allowing the mapping of elements, we want to be able to detect the signal of the metal that is linked to the protein studied, and thus to determine the localization of the protein in the sample being analysed.

The labelling with antibodies is called an immunolabelling and can be direct or indirect (see Figure 1):

- In the first case, the protein of interest is labelled with an antibody that is itself directly linked to a label (e.g., a fluorescent probe in the case of immunofluorescence, or with a chemiluminescent molecule in the case of chemiluminescent labelling, or metallic NP for the application of this work).

- In the second case, the use of a primary antibody and a secondary antibody is necessary. The primary antibody targets the protein while the secondary antibody carries the marker and is complementary to the primary antibody.

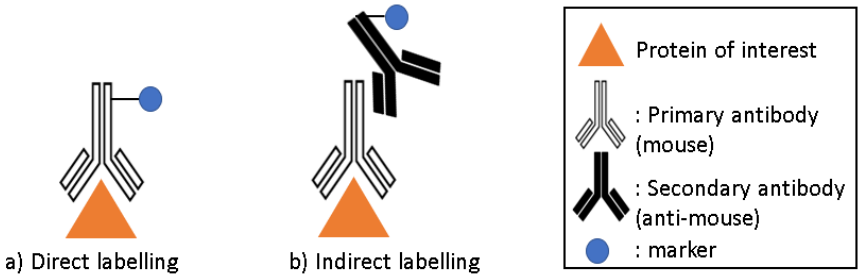


*Figure 1: Representation of a) a direct labelling using only one antibody that is linked to a marker and b) an indirect labelling, using a primary and secondary antibody.*

Since the primary antibody must recognise a particular protein, it has a high degree of specificity. The secondary antibody, on the other hand, can be more versatile, because it only has to be characteristic of the animal species that produced the primary antibody. The complementarity between the primary and secondary antibodies is illustrated on Figure 1b. The protein of interest that was used is the involucrine. It was chosen because it is a protein that is normally located in the stratum corneum, the uppermost layer of the epidermis. If the labelling with the nanoparticles works, the signal of the metal should be colocalized with organic signal coming from the stratum corneum, which is typically free fatty acids.

For this labelling, a gold NP (AuNP) was used as a marker. Thanks to its high sputtering and ionisation yield, gold is known to give rise to an intense signal in ToF-SIMS. The NPs that were used were produced via magnetron sputtering, a physical vapor deposition technique.

Due to the will of creating a versatile and cost-effective method, the indirect immunolabelling was chosen. Indeed, by carrying out an indirect labelling, there is only a need to change the primary antibody to target a different protein, while keeping the same secondary antibody, provided that it is compatible with the animal species of the primary antibody. The financial aspect is also not negligible. Indeed, secondary antibodies are polyclonal antibodies, they are less specific and thus less expensive than primary antibodies. During the process of binding the antibody to the nanoparticle, the reaction efficiency is not optimal and a certain amount of antibodies is lost, making it more advantageous to use low-cost antibodies.

The objective of the project was therefore to be able to perform indirect immunolabelling of proteins of interest in reconstructed epidermis in vitro, using AuNPs and then detect the signal of these AuNPs in ToF-SIMS.

The epidermis corresponds to the very last layer of skin cells we have. It is a dynamic system constantly evolving and renewing itself. It protects the organism from harmful substances and limits water loss. The structure of the epidermis is represented on Figure 2. There are four distinct histological layers: the stratum basale (SB) is which keratinocytes (the main type of cell of the epidermis) are formed, the stratum spinosum (SP), the stratum granulosum (SG) and the stratum corneum (SC). The keratinocytes, once produced in the SB, are continually moving up to higher layers. They differentiate and undergo cornification (final state of differentiation) [5] and their morphology changes too [6]. This is a homeostatic system, which means that it is at equilibrium. Indeed, there in a balance between the cells created in the SB and the ones that are lost via desquamation in the SC. The epidermis contains other species than keratinocytes, like Merkel cells, Langerhans cells, or melanocytes for the production of pigment. However, keratinocyte is the main type of cell in the epidermis [6].

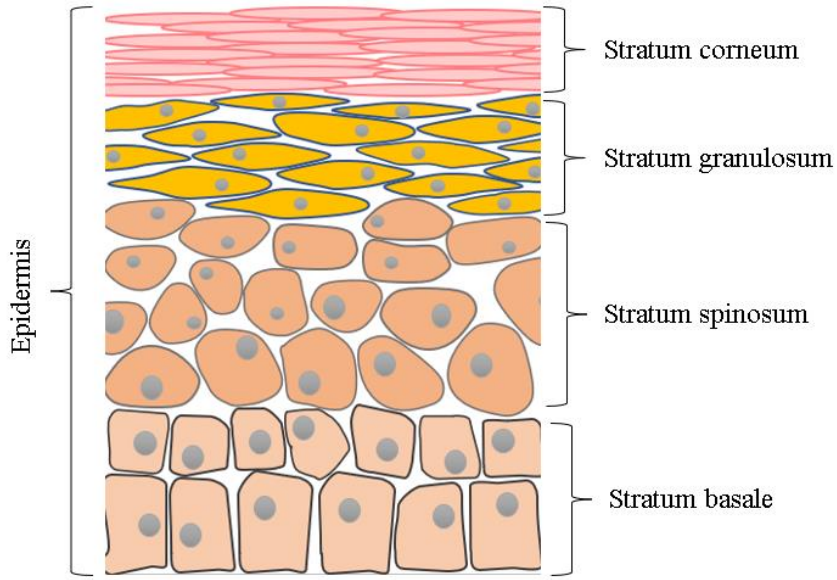


*Figure 2 : Schematic representation of the histological layers of a simplified epidermis. Stratum basale is the first histological layers composed of basal keratinocytes which differentiate to compose the stratum spinosum, stratum granulosum and finally the stratum corneum.*

This work is based on the results of experiments performed last year in the context of this project. During these early steps, PPAA-coated AuNPs were produced by PVD and characterized by TEM, AAS and ToF-SIMS. They were then conjugated to anti-mouse polyclonal antibodies using a protocol adapted from a patent filed by the University of Namur, based on the work of researchers at the LARN [7] [8]. This year, we seeked to deepen these results by applying the antibody-NP conjugates to the specific immunolabelling of epidermal proteins. The followed workflow involved several key steps. First, the ability of the conjugates to recognize and link to its target was assessed by performing an ELISA assay. Then, staining of reconstructed human epidermis was performed for immunofluorescence and ToF-SIMS analyses, in order to verify the immunolabelling that was performed. This required the adaptation of IHC protocols for labelling with this type of probe and also finding the appropriate ToF-SIMS analysis conditions for the detection of the AuNPs.

# 2. Materials and methods

## 2.1. ToF-SIMS

Figure 3 provides a representation of the main elements involved in a ToF-SIMS instrument. The primary ion beam is sent onto the sample and causes the sputtering of atoms and molecules from the surface, some of which are ionized and form so-called secondary ions [2]. An extraction voltage (2 kV) is applied between the sample and the extractor and a potential difference (positive or negative) induces an electric field that accelerates these secondary ions towards the time-of-flight analyser. The acceleration occurs over a region of a known length and with a velocity characteristic of their mass. By measuring the time taken for the ions to travel this distance, it is possible to obtain their mass/charge ratio (m/z) using the conversion equation below. It should be noted that electrons and photons are also ejected from the surface.

Ions velocity is given by : $v = \sqrt{\frac{2E_0}{m}}$

Time of flight is given by : $t = \frac{L}{v} = L\sqrt{\frac{m}{2E_0}} = k\sqrt{m}$

Time/mass conversion is given by : $m = k^{-2}t^2$

Where *m* is the mass of the ionised fragment, L the travelled length and $E_0$ its kinetic energy.

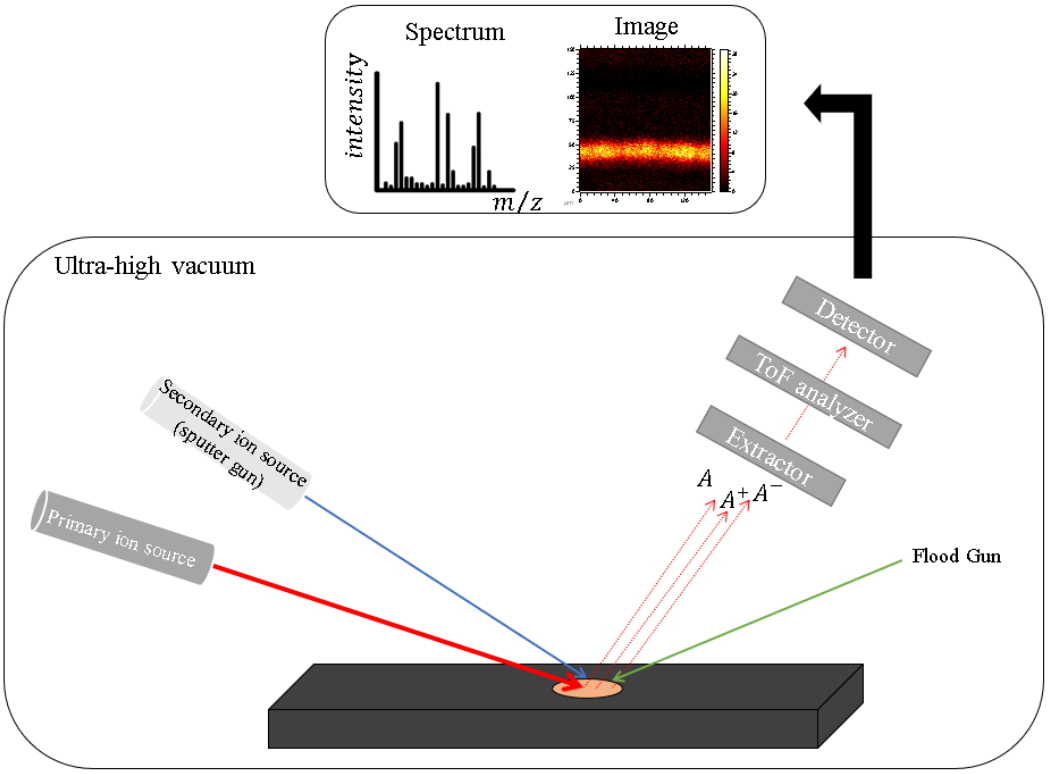


*Figure 3 : Schematic representation of a ToF-SIMS instrument. Analysis and sputtering beams are represented, as well as the charge compensation beam, the flood gun. Ejected species can be neutral or ionized, and the ions are collected then detected to form a mass spectrum as well as images.*

In terms of data acquisition, the ion beam probes the sample one pixel at a time, producing a mass spectrum for each pixel (see Figure 4). This allows the sample to be imaged and their composition mapped based on the intensity distribution of each SI peak.

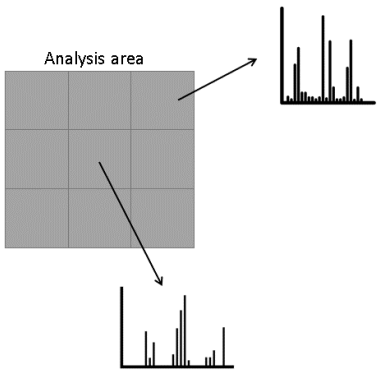


*Figure 4 : Schematic representation of the analysis area that is divided into pixels, each of which giving rise to a mass spectrum.*

It should be noted that when imaging is combined with depth profiling, it is possible to obtain 3D representations of the samples.

When using ToF-SIMS, surface charging can occur for insulating samples and can have an effect on the results observed. When the sample is bombarded, the ionization of atoms of the surface can lead to a net positive charge on the surface. Charge compensation is a solution to this problem and is achieved with a flood gun, which produces a beam of low-energy electrons.

The analysis is performed in an ultra-high vacuum environment, thanks to two connected chambers. The main chamber houses the beams and is where the analysis is conducted. The introduction chamber, also known as the airlock, is utilized to introduce samples into the main chamber without the need to vent, then pump down the high volume of the main chamber, thus saving time. The airlock chamber achieves a vacuum pressure of approximately $10^{-7}$ mbar, while the main chamber maintains a vacuum pressure of $10^{-9}$ to $10^{-10}$ mbar [9].

The analysis beam can be monoatomic ($Ar^+, Ga^+, Bi^+, \ldots$) or polyatomic ($Au_n^+, Bi_n^+, \ldots$) and is pulsed. The system used during this work is equipped with a bismuth Liquid Metal Ion Gun (LMIG). The source produces monoatomic bismuth ions and also clusters, both with the same energy but different velocities. The ones used for the analysis are selected thanks to a mass filter. The use of a polyatomic beam instead of a monoatomic beam depends on the purpose of the analysis and the type of sample. A monoatomic source presents a high beam current compared to polyatomic sources and allows the collection of atomic species or molecular fragments of a size limited to a few atoms. Polyatomic sources are preferred for organic samples as they deliver their energy to the surface softly compared to monoatomic ion sources and provide information with less deterioration of the samples [9, 10]. Moreover, it allows to preserve molecular information at high mass.

A typical analysis probes the very first atomic layers [9,10]. This type of analysis is called static SIMS, as opposed to dynamic SIMS, which uses a complementary ion source. This one is called the sputtering beam, in the sense that it is used to gradually etch the surface. In this case, the sputtering beam is used alternately with the analysis beam and the fragments ejected during the erosion phase are not analysed. A crater is formed when eroding and the analysis is performed on the freshly exposed layer, on a smaller area compared to the crater formed, in order to have the flattest surface, for instance 100x100 µm² against 500x500 µm². The Figure 5 represents the combination of the two beams and the formation of the crater.

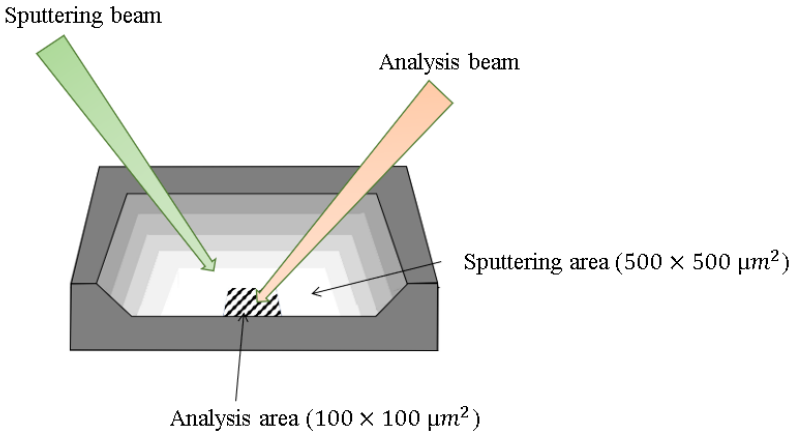


*Figure 5 : Schematic representation of the analysis and sputtering beams that are sent onto the analysed sample. The sputtering area is much larger than the analysis area in order to have a flat surface for the analyses.*

Regarding the sputtering beam itself, it can also be of different types. Monoatomic ions are used, such as $Cs^+, Xe^+, Ar^+$ or polyatomic, for instance $O_2^+$ or $Ar_n^+$ [9]. The extent of damage is directly proportional to the energy of the incident beam. Higher energy levels result in more significant damage. For organic samples analyses, low energy beams are preferred, in order to better preserve the covalent bond in the molecules. In fact, these links can be broken by an energy of around 30 eV.

Cesium and xenon have almost the same mass but different chemical reactivity [11, 12, 13]. Indeed, xenon is chemically inert and destroys the molecular information, it also has a low sputtering yield[1]. For cesium, things work differently. Indeed, it has a high reactivity and besides it has a low electronegativity. These features induce the improvement of the ionization by cesium, it has a reducing role, producing ions thanks to an oxidation-reduction reaction:

$$M + Cs \rightarrow M^- + Cs^+$$

This equation explains the improvement of the negative ionisation by cesium. When $Cs^+$ hits the surface, it is implanted in it and is neutralised to form Cs along with the free radicals that are created. These Cs block free radicals, unlike xenon, which prevents them from reacting with other substances. $O_2^+$ also reacts with the surface and increases the positive ionisation in the same way as $Cs^+$. Additionally, argon cluster sources have also been developed, where the atoms are linked by Van Der Waals bonds. These clusters induce a high sputtering yield and a high depth resolution. When hitting the surface, these atoms separate and the energy is distributed between each of them, inducing low energy impacts [10].

## 2.2. Synthesis of nanoparticles : magnetron sputtering

Nanoparticles (NP) are called so because of their size - they have dimensions in the nanometer scale. Due to this particularity, they exhibit unique optical, electrical and magnetic features that differ from the macro-objects. Their properties make them interesting for several applications, going from chemistry to medicine or electronics. Reference [14] gives an overview of the different types of NPs that exist and their applications. The applications in drugs and medications are indeed very important. NPs are used to increase the efficiency of certain drugs [15]. They are also used for imaging application, showing a good contrast in cells. Nanotechnologies are also being developed in the field of electronics, for instance with the use of nanoparticles in transistors or miniature chips [14]. In the case of this work, AuNPs were chosen for two reasons. First because of their ability to link to antibodies, according to the bioconjugation process described in section 2.4. Second, because of their high sputtering and ionisation yield, giving rise to an intense signal in ToF-SIMS, which make it easy to discriminate it from the organic component of the signal.

Different synthesis pathways exist nowadays, all having their own characteristics. In general, we classify the different pathways into biological, chemical and physical methods. The biosynthesis of nanoparticles takes advantage of organisms such as plants to synthetize them, in a clean and non-toxic way [16]. Plant extracts are used to reduce the gold ions into NPs [15]. The properties of the NPs depend on the plant that is used and on the reaction time. The use of microorganisms is also possible but is more expensive. On the other hand, chemical pathways allow the production of gold nanoparticles with better control of their size. However, they need toxic components for the reduction. The principle is based on reducing a gold salt through a

[1] Sputtering yield = number of atoms ejected per incidents atoms on the surface [10].

chemical agent which reacts with the metal ions and force them to aggregate and form nanoparticles [17, 18]. Finally, physical pathways exist.

Physical vapor deposition (PVD) appeared around 1920 and the magnetron sputtering technique was developed in the early 1970s. This technique uses no solvent but a plasma reactor, which makes it more environmentally-friendly than the previous ones. It is used for the growth of films on different substrate. It also allows coatings, which are widely used to give properties to engine components, for instance to reduce frictional forces and enhance the mechanical resistance [19]. This technique can also be used to improve performance and lifetime of medical devices [20]. It is indeed possible to modify the metal surface of the tools to avoid corrosion or improve biocompatibility. The nanoparticles used for this work were produced using a PVD system from AJA International. They have a core-shell structure in which a gold core with a mean diameter of 5,3 nm (previously determined by TEM) is surrounded by a poly-allylamine polymer shell, as shown on Figure 6.

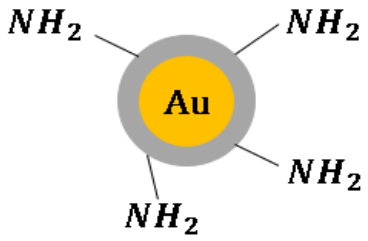


*Figure 6: Schematic representation of a nanoparticle of gold with a shell of polyallylamine. $NH_2$ functions are exposed to the outside of the nanoparticle.*

The system is composed of a vacuum chamber and two magnetron sputtering sources. The gold source and the substrate are positioned face to face in the chamber, with the source being brought to a negative potential. A sputtering gas, argon, is injected into the AJA and naturally ionized atoms are generated, for example by cosmic rays, forming a plasma near the target (a glass disk) [21]. This facilitates the pre-formation of nanoparticles. Due to the electrical field created in the chamber, positive ions are accelerated towards the target, hitting it and inducing a sputtering of atoms that will cross the plasma and reach the substrate [22]. The magnetic field, on the other hand, is added to confine electrons in a certain area of the plasma, near the target, increasing the probability of collision. The setup is illustrated in Figure 7, where the substrate is positioned on a rotating plate, enabling it to face the gold and NaCl sources simultaneously. In the magnetron sputtering AJA chamber, the substrate is positioned at a distance of 15 cm above the target. The process is carried out at a pressure of 180 mTorr, using a power of 74 W and a deposition time of 16 seconds for the gold layers. For the PPAA layers, the pressure is set to 60 mTorr, the power is 44 W and the deposition time is 40 seconds. The PPAA shell is not produced by magnetron sputtering, it is achieved by plasma polymerization of a monomer. Indeed, a bottle of liquid allylamine is connected to the chamber and allylamine vapor is injected and polymerize thanks to a carbon cathode. Without the functionalization of the nanoparticles, the transfer in aqueous solutions wouldn't be possible because of aggregation. This coating is also needed for the bioconjugation, as it will be explained later, the amino functions of polyallylamine will bind to the carboxyl functions of the antibodies.

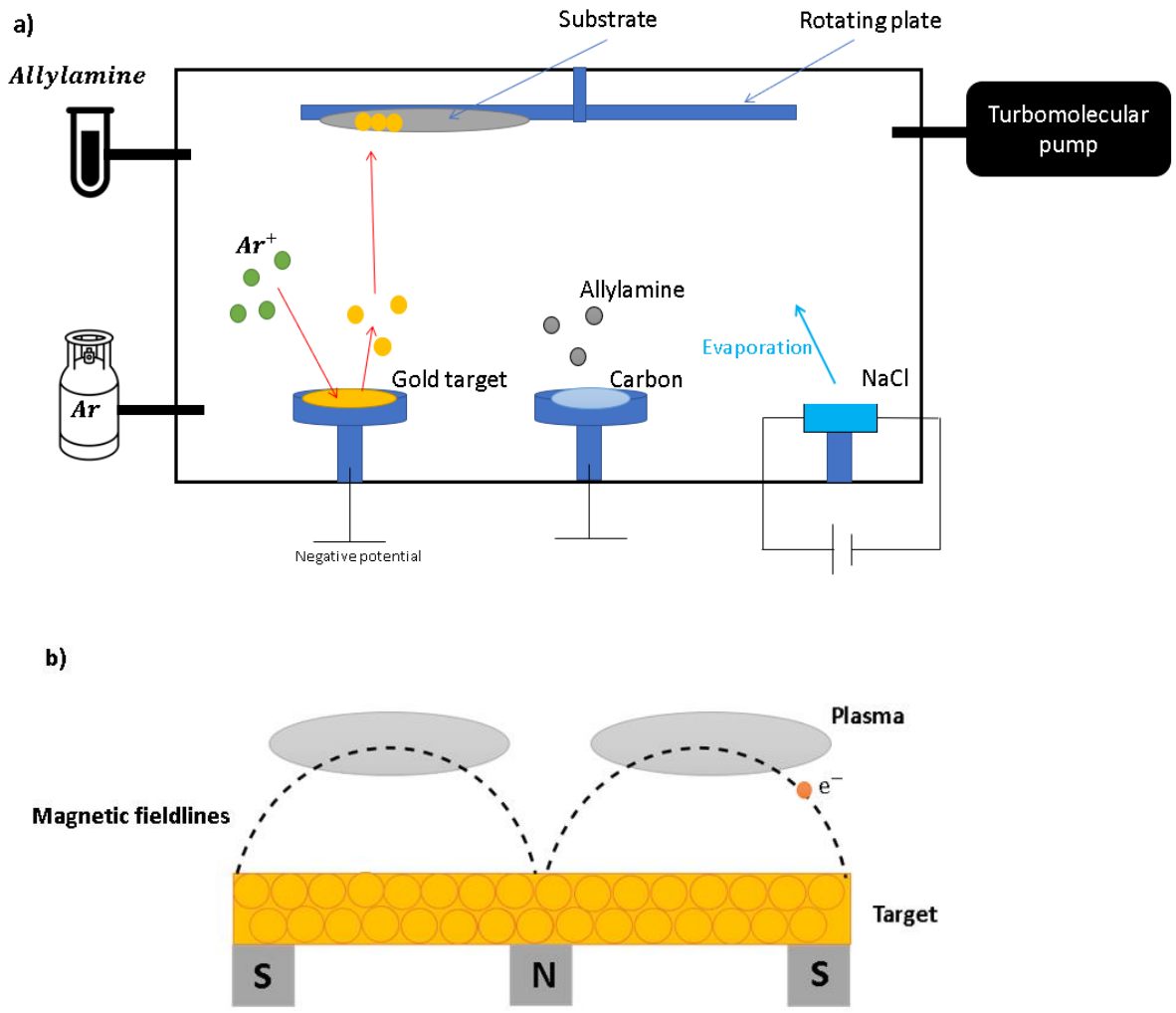


*Figure 7 : a) Schematic representation of the magnetron sputtering chamber that was used for the production of the gold nanoparticles and b) Schematic representation of the magnetic fieldlines and the plasma induced near the target.*

From a more practical point of view, the production of nanoparticles in the magnetron sputtering AJA chamber is realized through the stacking of 66 layers of gold NPs (see Figure 8). Each layer is sandwiched between PPAA layers, making PPAA-NP-PPAA sandwiches, themselves enclosed between NaCl layers. The NaCl is later dissolved and acetic acid is added to the solution. This allows the protonation of amine groups of the polymer coating, leading to an electrostatic repulsion between AuNPs, which enables their separation [23]. Finally, the resulting colloid is purified through centrifugal diafiltration in order to remove $Na^+$ and $Cl^-$ ions, as well as polymer debris and other impurities.

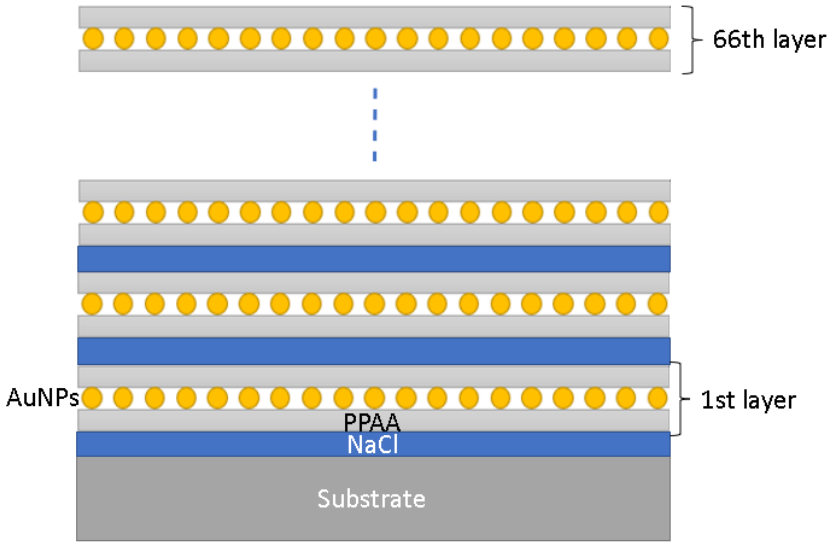


*Figure 8: Schematic representation of the layering of gold nanoparticles, PPAA layers and NaCl. There are around 66 layers formed during the hole process of nanoparticles formation.*

## 2.3. Nanoparticles characterization with ToF-SIMS

The NPs produced were characterized by transmission electron microscopy and atomic absorption spectroscopy (see below for details) last year, for the research project of master 1. The NPs were also analysed with ToF-SIMS.

Analysis were performed on the back-mounted sample holder, using a liquid metal ion gun (LMIG) made of bismuth, producing 25 keV $Bi^{3+}$ and a current of 0.25 pA. Raster size was 500x500 µm² for 110 scans and a cycle time of 150 µs. Spectra were acquired in negative polarity. For each measurement, the floodgun was activated, with a current of 2,35 A, whose role is to compensate for electrical charges resulting from the ejection of ions from the surface. Charge compensation was also improved by adding argon flooding in the main chamber, at a pressure of around $5.10^{-7}$ mbar.

Although gold nanoparticles present a high sputtering yield and a high ionisation yield with ToF-SIMS, the ones used for this master thesis are coated with a polymer that could influence the signal and the characteristic fragments generated from the AuNPs. This characterization aims to assess which fragments could be used to track the position of the AuNPs on a labelled tissue cross section.

Regarding the sample preparation, the AuNPs solution is diluted from 1 to 1:1000000 and a drop is deposited onto a silicon slice. The drops were then dried in a 70°C oven and the samples were degassed under vacuum in an introduction chamber prior to analysis. The purpose of this measurement is thus to determine the detection limit.

## 2.4. Bioconjugation reaction

The conjugation of the AuNPs to antibodies is a crucial step in tagging proteins of interest with nanoparticles. The use of antibodies is widespread in different fields of sciences, not only in biology. For instance, the combination of antibodies with radionuclides can be used for radioimmunotherapy [24] and a combination with a probe is very used in biological assays such as ELISA assay or western blotting.

Several ways for functionalizing nanoparticles exist, some of them use the carbodiimide chemistry, which is expensive, toxic and time-consuming. The LARN recently developed and patented a protocol for a new bioconjugation technique [7], using a coupling molecule called COMU[2]. This technique conjugates AuNPs to an antibody (Cetuximab for them) in a faster and more environmentally friendly manner, using less toxic compounds and using suspensions in Phosphate Buffered Saline (PBS), which is easier for biological applications. This technique is also less expensive than the previous ones and requires few steps [25].

This technique takes advantage of the amine functions of the PPAA shell of the NPs and use the COMU to establish the amide link between the amino functions of the nanoparticle and the carboxyl functions of the antibodies [25, 26], as shown on Figure 9.

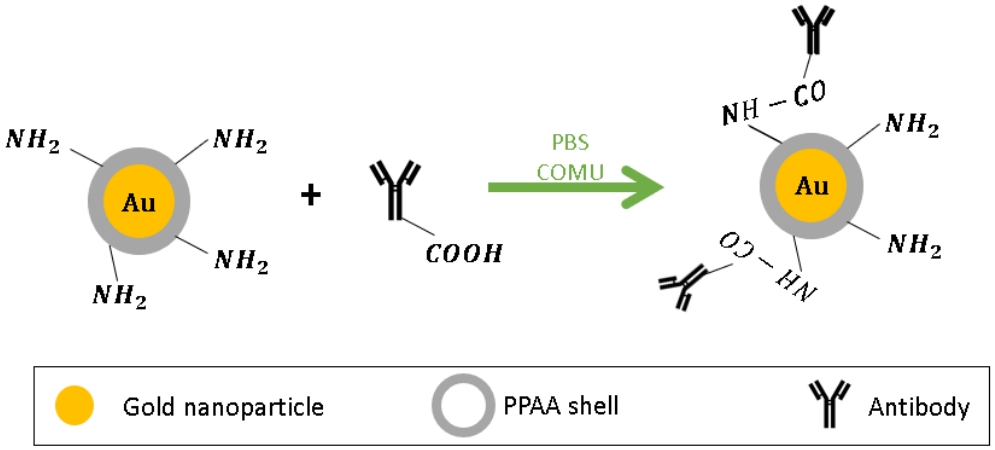


*Figure 9 : Schematic diagram of the bioconjugation between gold nanoparticles and antibodies. The nanoparticles coated with the allylamine polymer are linked to antibodies in a solution with PBS, via the use of a coupling molecule, the COMU.*

A solution of COMU is mixed with a solution containing the antibodies. The antibodies used for the bioconjugation are polyclonal anti-mouse antibodies from Novex (life technologies), as the primary antibody is produced by a mouse. The AuNPs colloid is then added to the mixture to complete the bioconjugation.

Purification is necessary to obtain a pure solution and get rid of unconjugated antibodies. This is achieved through a centrifugal diafiltration, during which the PBS used for each solution is evacuated and replaced by milli-Q water. The bioconjugate is centrifuged in Vivaspin centrifugal concentrators of 6 mL, with a MWCO[3] of 300 kDa. The use of semi-permeable membranes allows separating of species in solution. Changing the solvent is useful to eliminate macromolecules that could pollute the retentate. The diafiltration must be repeated several cycles until filtrate conductivity reaches that of water, indicating that the purification is complete.

[2]COMU=(1-Cyano-2-ethocy-2-oxoethylidenaminooxy)dimethylamino-morpholino-carbenium hexafluorophosphate

[3] MWCO = molecular weight of cut-off of the membranes of the concentrators, this defines what can pass through the filter or not.

## 2.5. Bioconjugate characterizations

### a) Atomic absorption spectroscopy

AAS (Atomic Absorption Spectroscopy) is a spectroscopic technique based on the well-known phenomenon of optical absorption in physics. It is used to determine the concentration of a metal ion in solution. In this case, it is the amount of gold in the AuNPs colloid that is sought. The sample to be analysed must be mineralised and the AuNPs are first diluted in a solution of aqua regia in order to convert the AuNPs into ions. The solution thus formed is absorbed by a capillary and atomised by an air/ethylene flame (this is called "Flame Atomic Absorption Spectroscopy"). The atomised sample is then illuminated with monochromatic radiation. The transmitted intensity is measured and an absorbance spectrum is obtained, as shown on Figure 10. This absorbance measurement can be directly related to the concentration by means of a prior calibration using standard solutions of known concentrations [27].

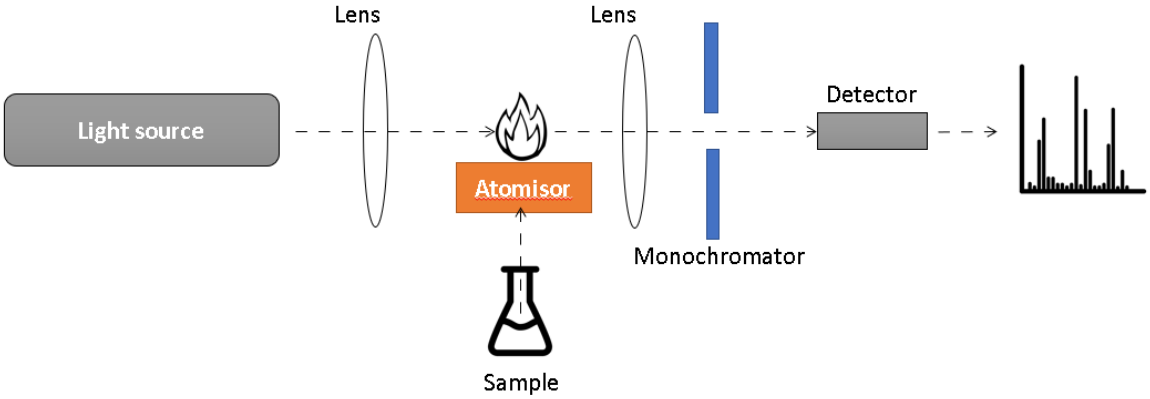


*Figure 10 : Schematic representation of atomic absorption spectroscopy, used to determine the metal concentration of a solution.*

### b) Pierce Assay

The Pierce assay is a colorimetric technique used to determine the concentration of antibodies in a solution [28]. To perform the assay, a reactive “Pierce reagent” is added to the solution and its absorbance is measured at 660 nm. The principle of that assay is that Pierce reagent binds to proteins, forming a complex that will induce a color-shift of the solution. When unbound, the reactive is red, but bound to a protein, the color of the complex turns greenish and displays an absorbance peak at 660 nm. Calibration is realized with standard solutions prepared with BSA diluted in milli-Q water and a blank of milli-Q water must be taken. The higher the protein concentration, the greener the solution and the higher the absorbance. A representation of this assay is provided on Figure 11. It should be noted that the contribution to the general absorbance due to the presence of AuNPs was also considered and eliminated for the calculation of the protein concentration.

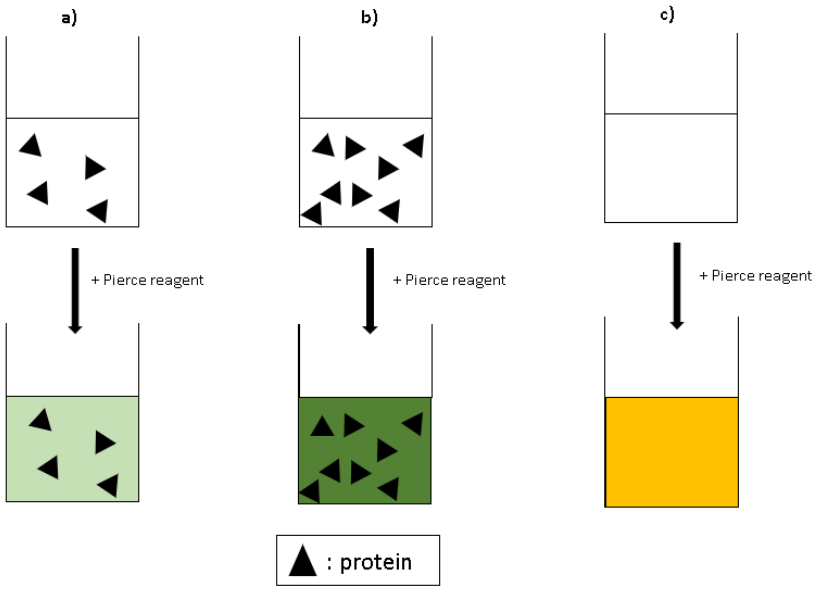


*Figure 11 : Schematic representation of the Pierce assay. A color-shift of the solution is observed when proteins are present. The color-shift cans be light (a) when few proteins are in solution and can be more intense when a lot of proteins are present in solution (b). If no proteins are in solution, Pierce reagent give an orange-red coloration to the solution (c).*

### c) ELISA assay

Enzyme-Linked Immunosorbent Assay (ELISA) is a technique designed for quantitative measurements of antigens and antibodies in a solution, using antibodies as the probe [29, 30]. This is typically used in pregnancy tests, or for HIV diagnosis for instance. Different types of ELISAs exist and the use of one instead of another depends on the application and the sensitivity of the system. The basis of this assay is the use of antibodies conjugated to enzymes, which, once in contact with their substrate, will induce an enzymatic reaction that produces a detectable color. A measurement with a microplate reader allows to measure the binding of the antibody with its antigen. The Table 1 represents the different types of ELISA and their functioning. The direct ELISA (a) is the case when the antigen of interest is fixed on the bottom of the well and a primary antibody, conjugated to an enzyme, is added. Then, the substrate for the enzyme is added as the last step of the ELISA. The term indirect ELISA (b) is used when a second antibody is used. The primary antibody is unconjugated and it is the secondary antibody that is linked to an enzyme and will produce the signal when the substrate is added. In the configuration of a sandiwch ELISA (c), the well is coated with an antibody and not the antigen. The second step is the adding of the antigen, that is going to bind to the antibody. A detection antibody is added, just before the conjugated antibody. Lastly, as in the other configurations, the substrate is added.

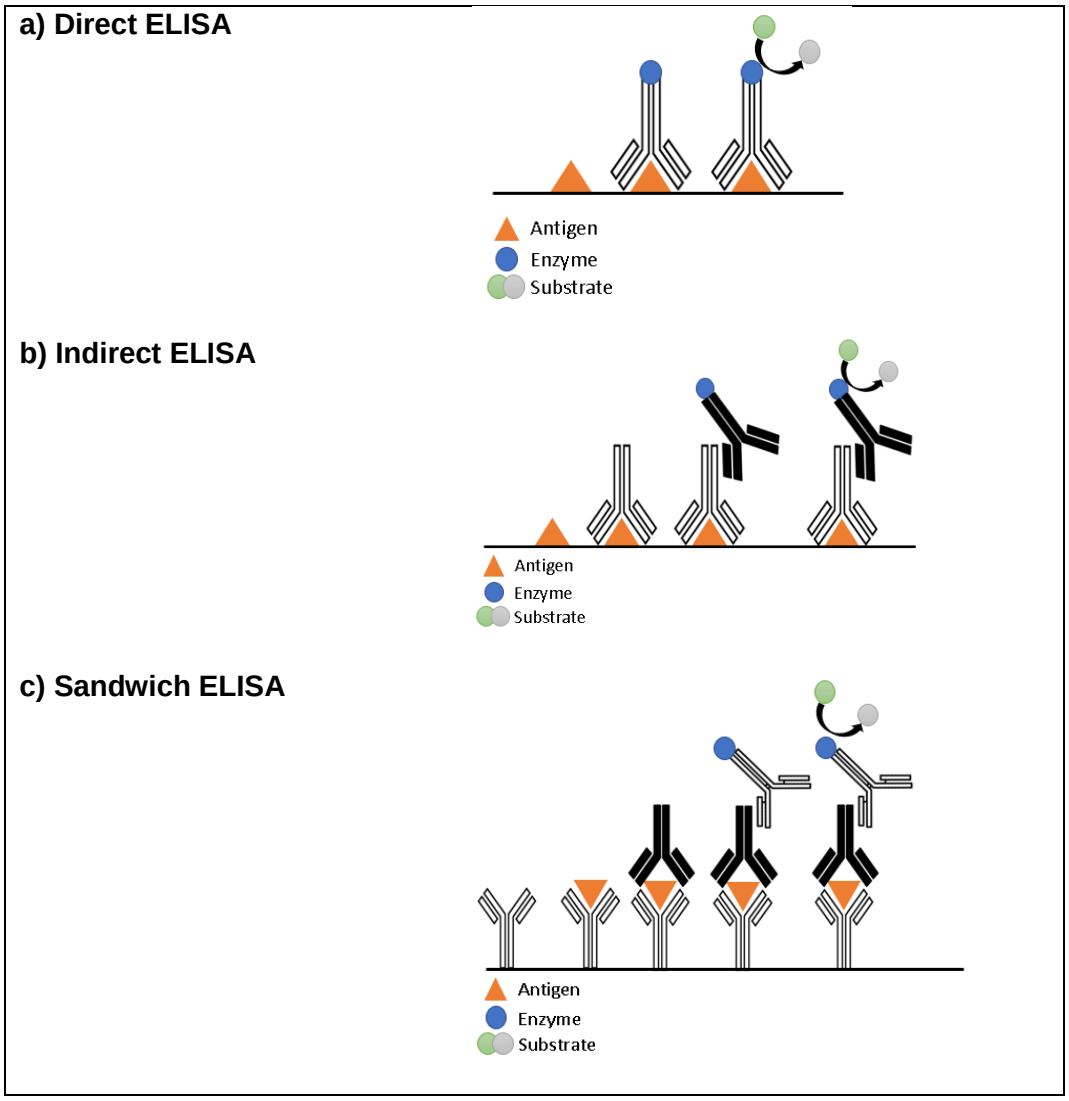


*Table 1 : Schematic representation of the direct ELISA (a), the indirect ELISA (b) and the sandwich ELISA (c). The figures are adapted from [29].*

It should be noted that the antigen or antibody is fixed to the ELISA plate thanks to COOH-link with the polystyrene plate (source article biotin-streptavidin). Like many biological assays, the protocol can be adapted to the needs of the experimenter depending on what is to be emphasized. In the case of this master thesis, the purpose was to determine whether the antibody conjugated would still be able to recognize its target after the bioconjugation process. Having undergone many chemical reactions during the bioconjugation, it is not guaranteed that the antibody kept its ability of recognition. To determine this, the ELISA was pursued as shown in Figure 12. The capture antibody (mouse anti-involucrine) covers the surface of the wells. The bioconjugated antibodies produced in the LARN are added and bind themselves to the target antibody. As a last step, the enzyme-conjugated antibody is added (donkey anti-goat antibody conjugated to biotin, Abcam). Here, biotin was used as enzyme and streptavidin-HRP is used as its substrate. Streptavidin is a tetrameric molecule, having 4 binding sites for biotin. When added in the wells, the streptavidin links to the biotin and the HRP provides an enzymatic activity. Streptavidin is often used in ELISA as it allows to amplify the signal of the assay.

Between each step, wells are washed with PBS to ensure that any unbound AC is removed from the system. If the antibodies conjugated to AuNPs are able to detect their target, then they

will not be washed out and will allow a signal as the biotinylated antibody is able to tag it. If no signal is observed, it means that the antibodies did not link to the target and were eliminated through the washings. Note that a positive and negative control are done to verify the accuracy of the results.

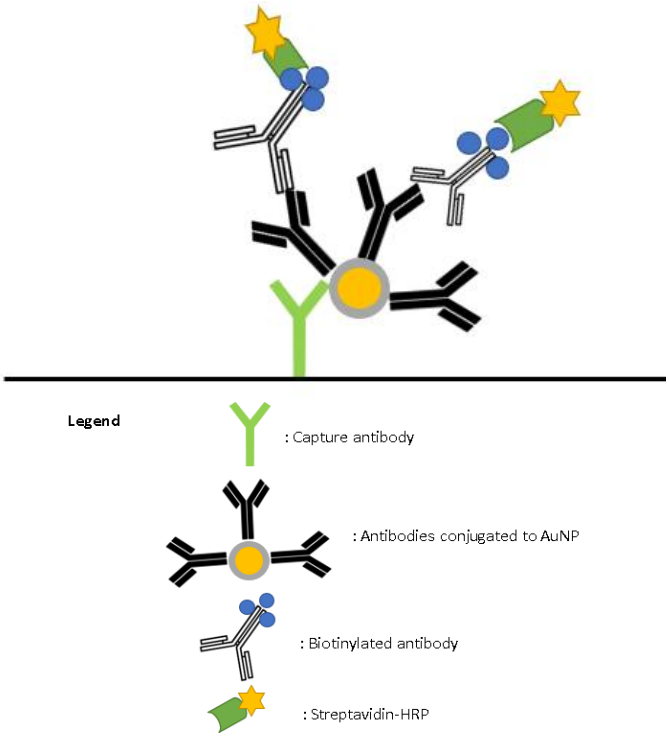


*Figure 12 : Schematic representation of the ELISA assay that was realised.*

### d) UV-vis spectroscopy

This technique uses a spectrophotometer to measure the optical absorbance of a liquid sample in a range from UV to visible (190 to 1100 nm). The intensity of light that passes through the sample is measured and is compared with a reference [31]. It is possible to measure a shift in wavelength of the localized surface plasmon resonance (LSPR) of the AuNPs, normally located between 500 and 600 nm, at different time to determine their stability [32].

## 2.6. Reconstructed human epidermis

This section aims to describe the model of the reconstructed human epidermis (RHE) that was used for this work. The use of explants of human epidermis being very restricted due to ethical reasons, a lot of different synthesis pathways are developed in order to produce in vitro human epidermis. Commercially available models of human skin are available but are very expensive and thus not affordable for academic laboratories [33]. The reference [33] offers a procedure open to everyone in order to produce reconstructed human epidermis with characteristics of the human epidermis. This section aims to give an accurate summary of the process that has been used for the master thesis, regarding the production of the RHE.

### a) Synthesis of RHE

As told earlier, RHE can be synthetized in a simple way. For more details about sample preparation, the reader is referred to the latter. The samples were prepared in the LabCeTi (Laboratoire Cellules et Tissus) at the UNamur. A skin sample is collected (with consent) during surgery and isolated keratinocytes are obtained thanks to the incubation in trypsin solution and the separation of the epidermis and dermis. The cells are centrifugated and resuspended in culture flasks to obtain a stock of keratinocytes. Then, keratinocytes obtained are seeded on a porous polycarbonate filter, with a cell density of around 250 000 $cells/cm^2$ [34]. The culture is done under submerged conditions during 24 hours, to allow the sedimentation and adhesion of the keratinocytes from the culture medium to the filters. After that, the culture is exposed to air so cells can continue to differentiate and stratification, forming the different layers of the epidermis. The cells are fed through the pores of the polycarbonate filter at the bottom of the well. It allows nutrients and oxygen diffusion but prevents keratinocytes from leaving the well, the pores having a diameter of around 4 µm. The culture medium that was used is the Epilife medium. It is a serum-free, low calcium medium, containing growth factors, hormones and nutrients and it is particularly efficient for the differentiation of keratinocytes. In addition to the Epilife medium, human keratinocyte growth supplement is used and the solution contains 1,5 mM $Ca^{++}$ and vitamin C. Calcium is added because it improves proliferation of keratinocytes and induces intercellular junctions [33] and several studies demonstrate that that calcium is a regulator of choice for the epidermal differentiation. However, further studies showed that the multiplication rate of keratinocytes depends more on cell density than calcium concentration [6]. Regarding vitamin C, it improves barrier properties of RHE, because it improves the lipid composition in the SC. In the end, fully differentiated RHE are obtained 11 days after seeding, replacing the culture medium every 2 days. In our case, we let the RHE grow for 13 days, in order to increase their thickness to around 90 µm, which allows for a better visualization of the different histological layers in ToF-SIMS. Figure 13 represents the setup of the reconstruction of an epidermis in vitro.

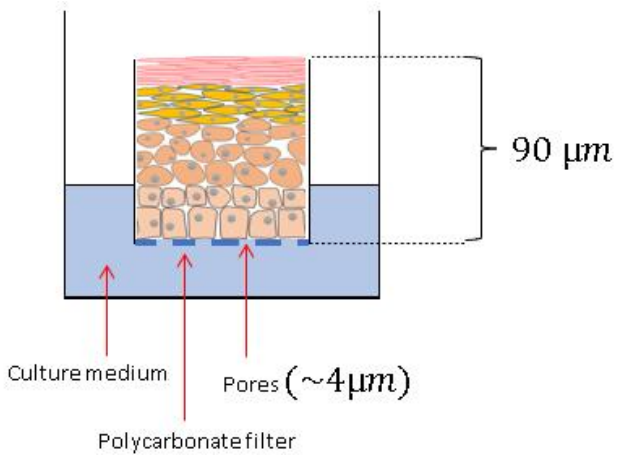


*Figure 13 : Schematic representation of the growth of the reconstructed human epidermis in vitro. The RHE obtained is around 90 µm thick and is obtained after 13 days of grow.*

### b) Sectioning and sample preparation

Once the RHE is produced, the next step is to embed it in Optimal Cutting Temperature (OCT) resin block before further processing. OCT is a water-soluble embedding medium

compatible with cryosectioning, i.e. the extraction of cross sections, around 10 µm thick, from a frozen tissue using a microtome. Sectioning is done at -10°C or below. The OCT is often used for immunofluorescence staining, as it leaves no residue on the slides, an important feature in order to avoid noise background. OCT can be frozen at temperatures going from -20°C to -80°C [35]. The RHE is extracted from the wel insert and takes form of a small disk that includes the polycarbonate filter and the various layers constituting the RHE. It is placed at 90° in a mold containing the OCT resin, which is dipped in methanol cooled to -80°C (see Figure 14). This allows the OCT to solidify and the mold is then placed in a freezer at -80°C. Once the OCT block is completely solidified, it is unmolded and pressed on a support with a drop of OCT in the center. This support is placed in the cryostat in order to maintain the sample at a low temperature. The cryostat is used to cut thin slices thanks to sharp blades. The thickness is controlled precisely and the sections are around 10 µm thick.

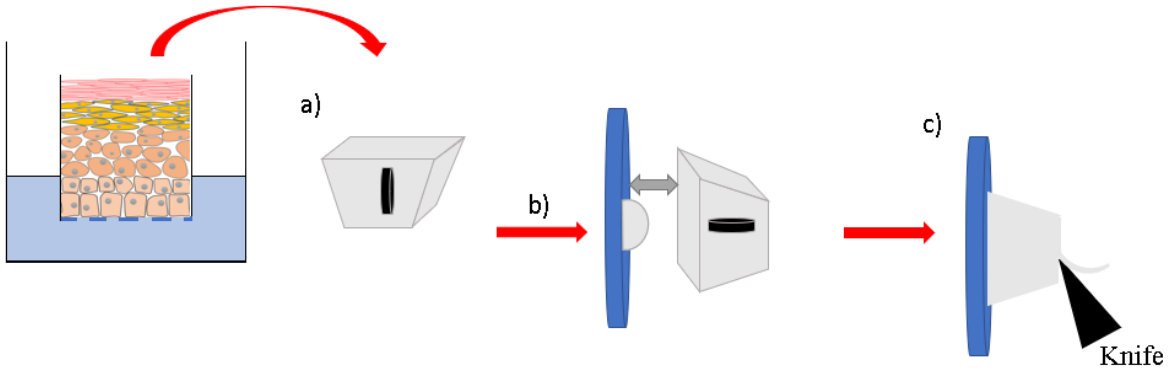


*Figure 14 : Schematic representation of the embedding step in OCT and cutting of cross sections. The RHE is removed from the insert (a) and is placed perpendicularly in a mold filled with OCT resin. The mold is immerged in methanol to solidify OCT resin. Once solidified completely and after being placed in a freezer at -80°C, the OCT block is unmolded and pressed on a support with a drop of OCT to allow the link (b). The support is placed in the cryostat, to cut cross sections of RHE with a knife (c).*

The epidermis sections are placed on three different supports, depending on the required analysis :

- Silicon substrates of 1,5cm x 1,5cm, containing one section of RHE. This substrate is used for the ToF-SIMS control analysis of the unmarked RHE, in order to determine the characteristic peaks of the epidermis;
- *SuperFrost Plus Adhesion* slides [36], with 3 sections of RHE on each. This is a type of glass microscope slide that is coated with silane to improve adhesion of RHE sections. This type of substrate was used for several purposes. First of all, to control the cross sections thanks to optical microscopy as they should be as straight as possible. Those slides were also used for staining experiments. Indeed, during staining steps, one must immerge the slides in several solutions, which can lead to a loss of the RHE on the slide. Thanks to this specific coating, the RHE has a better adhesion. Those slides are also used for the fluorescence microscopy, as we marked the RHE with the bioconjugate but also with fluorescence label. ToF-SIMS analysis were made, with the top mounted sample holder.
- Silicon substrates coated with silane, by being immerged in acetone and aminopropyltriethoxysilane, of 1,5cm x 1,5 cm, containing one section of RHE. They are also used for staining experiments for ToF-SIMS analysis. Thanks to their small size, it is possible to use the back-mounted sample holder, which allows the analysis of more RHE sections at the same time.

### c) Staining of the RHE sections

The stainings of the RHE cross sections were achieved according to immunohistochemistry protocols with two different probes. On the one hand, fluorescent antibodies were used for immunofluorescence experiments. The sections stained with a fluorescent probe were analysed with a fluorescence microscope in order to verify the binding of the primary and secondary antibody and ultimately, give a confirmation of the ToF-SIMS results with a well-known and optimized methodology. For the ToF-SIMS analyses, the fluorescent probe is replaced by AuNPs and their signal is detected in ToF-SIMS.

The immunohistochemistry assay was achieved in the LabCeTi once again, after several adaptations of a protocol routinely used. Indeed, the protocols are designed for fluorophore-labelled antibodies, the concentrations are set for this type of probe and must be adapted for AuNPs. First of all, the sections of RHE must be air-dried for around 30 min to 1 hour and immersed in neutral formalin for 10 minutes. This is a fixative commonly used in histology [37] to preserve the structure and morphology of the sample. It prevents cell degradation. PBS is used to rinse the samples - for 5 minutes three times in a row. A second rinse is performed to eliminate any remaining aldehyde, using glycine 0,1M in deionized water, for 5 minutes. This compound is a small amino acid that binds free aldehyde groups to prevent them to bind to the antibodies. The next step consists in the permeabilization of the cellular membranes and the reduction of background noise, using a detergent, Triton X100 (0,1%) and a solution of PBS containing Bovine Serum Albumin (BSA). BSA, is a blocking agent used to avoid non-specific bindings of the antibodies. This is done during one hour and the incubation with primary antibody, which is also diluted in PBS-BSA-triton, is performed for the same duration. PBS-BSA-detergent is used again to rinse 3 times 5 minutes before the secondary antibody incubation. For the verification of the ACAuNPs link, a third incubation is needed with a fluorescent antibody that binds to the ACAuNPs. Table 2 sums up the different staining experiments.

It should be noted that the cross sections designed to the fluorescence microscopy were also incubated with DAPI, which is a fluorescent component that penetrates into the cells to mark the nucleus. It will allow to visualise the nucleus in the RHE section. Technically, the signal should only be visible in the first layers of the RHE and not in the stratum corneum, as the cells in this layer do not have a nuclei.

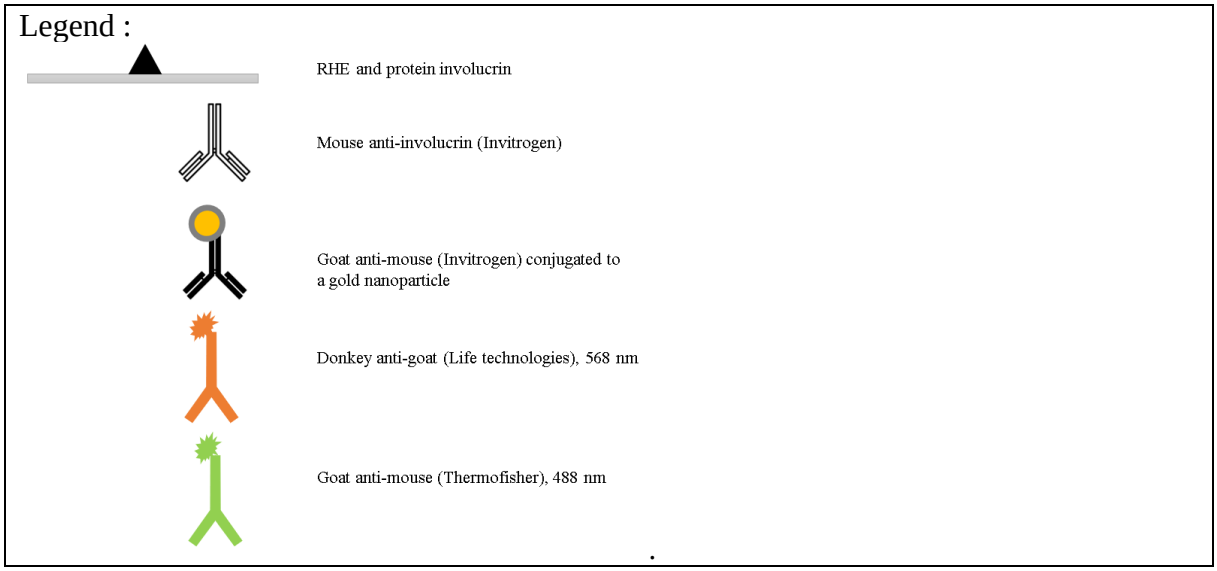

| | |
|---|---|
| ToF-SIMS measurements | |
| 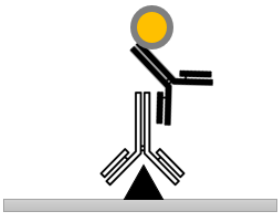 | Experimental setup destined for ToF-SIMS analysis, to verify the detection of gold signal. The concentration was varied during the experiments, with dilution factors of 100x, 200x and 400x. The primary antibody is a mouse anti-involucrin and secondary antibody is the ACAuNPs produced in the LARN. |
| 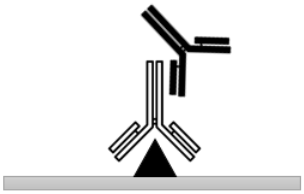 | Negative control setup using unconjugated antibodies. The secondary antibody is also the goat anti-mouse but unconjugated. |
| Immunofluorescence measurements | |
| 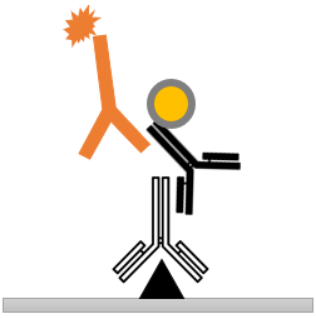 | Verification of the fixation of the conjugated antibody. Three incubations are needed for this condition. The primary antibody is the same as previously, and is targeted by the ACAuNPs as secondary antibody. A third incubation must be done with the fluorescent antibody, to detect the fluorescence with the microscope. |
| 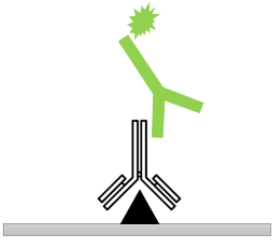 | Verification of the fixation of the primary antibody to its target. Only the primary antibody and the secondary fluorescent antibody are used. |
|  | Control setup. Verification of non-specific fixation of the detection antibody, in order to remove the background fluorescence. Once again, only primary antibody and secondary fluorescent antibody were used. |

| | |
|---|---|
| 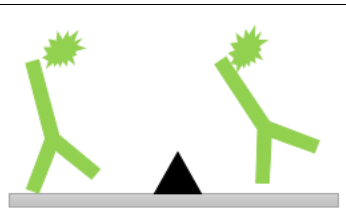 | Control setup. Verification of non-specific fixation of the detection antibody, in order to remove the background fluorescence. This condition only requires one incubation with the fluorescent antibodies. |

*Table 2 : Summary of the staining experiments that were done on the RHE, for immunofluorescence and ToF-SIMS analyses.*

## 2.7. Analysis conditions with ToF-SIMS

This subsection sums up the analysis condition of each sample probed with ToF-SIMS. Data calibrations applied to each sample are also provided in this section.

| **Sample 1 : AuNPs deposited onto silicon substrate, related to AuNPs characterizations** | |
|---|---|
| **Analysis parameters** | |
| Polarity | Negative |
| Primary ions | $Bi_3^+$ |
| Energy | 25 keV |
| Area | (500 µm)² |
| Stop condition | 110 scans |
| Sample holder | Back mounted |
| **Mass calibration list** | |
| **Ion** | **Mass (amu)** |
| $C_2^-$ | 24.000549 |
| $C_4^-$ | 48.000549 |
| $Au^-$ | 196.967101 |
| $Au_3^-$ | 590.900205 |
| $Au_5^-$ | 984.833309 |
| **Sample 2 : Control RHE deposited on superfrost+ substrate, without any labelling steps** | |
| **Analysis parameters** | |
| Polarity | Negative |
| Primary ions | $Bi_3^+$ |
| Energy | 25 keV |
| Area | (100 µm)² |
| Stop condition | 60 scans |
| Sample holder | Top mounted |
| **Mass calibration list** | |
| **Ion** | **Mass (amu)** |
| $CH^-$ | 13.008374 |
| $OH^-$ | 17.003288 |
| $CN^-$ | 26.003623 |
| $C_{18}H_{33}O_2^-$ | 281.248604 |
| $C_{24}H_{47}O_2^-$ | 367.358154 |
| $C_{26}H_{51}O_2^-$ | 395.389454 |
| $C_{27}H_{45}SO_4^-$ | 465.304404 |

| Sample 3 : Labelled RHE deposited on superfrost+ substrate | |
|---|---|
| **Analysis parameters** | |
| Polarity | Negative |
| Primary ions | $Bi_3^+$ |
| Energy | 25 keV |
| Area | (100 µm)² |
| Sample holder | Top mounted |
| **Sputter parameters** | |
| Sputtering beam | $Cs^+$ |
| Energy | 0.50 keV |
| Crater size | (450 µm)² |
| Sputtering time | 8s + 1s pause |
| **Mass calibration list** | |
| **Ion** | **Mass (amu)** |
| $C^-$ | 12.000549 |
| $CH^-$ | 13.008374 |
| $CH_2^-$ | 14.016199 |
| $OH^-$ | 17.003288 |
| $C_2N_2Au^-$ | 248.973249 |
| $Au_3^-$ | 590.900205 |
| **Sample 4 : Labelled RHE deposited on silicon substrate** | |
| **Analysis parameters** | |
| Polarity | Negative |
| Primary ions | $Bi_3^+$ |
| Energy | 25 keV |
| Area | (150 µm)² |
| Sample holder | Back mounted |
| **Sputter parameters** | |
| Sputtering beam | $Cs^+$ |
| Energy | 0.35 keV |
| Crater size | (500 µm)² |
| Sputtering time | 6s + 1s pause |
| **Mass calibration list** | |
| **Ion** | **Mass (amu)** |
| $C^-$ | 12.000549 |
| $CH^-$ | 13.008374 |
| $CH_2^-$ | 14.016199 |
| $OH^-$ | 17.003288 |
| $C_2N_2Au^-$ | 248.973249 |
| $Au_3^-$ | 590.900205 |
| **Sample 5 : Control for labelled RHE with unconjugated antibodies** | |
| **Analysis parameters** | |
| Polarity | Negative |
| Primary ions | $Bi_3^+$ |
| Energy | 25 keV |
| Area | (120 µm)² |
| Sample holder | Back mounted |

| Sputter parameters | |
|---|---|
| Sputtering beam | $Cs^+$ |
| Energy | 0.35 keV |
| Crater size | (500 µm)² |
| Sputtering time | 6s + 1s pause |
| **Mass calibration list** | |
| **Ion** | **Mass (amu)** |
| $C^-$ | 12.000549 |
| $CH^-$ | 13.008374 |
| $CH_2^-$ | 14.016199 |
| $C_2H_3$ | 27.024024 |
| $C_{14}H_{11}O_2^-$ | 211.076453 |
| **Sample 6 : Control for labelled RHE without primary antibody, verification of the specificity of the labelling with ACAuNPs** | |
| **Analysis parameters** | |
| Polarity | Negative |
| Primary ions | $Bi_3^+$ |
| Energy | 25 keV |
| Area | (120 µm)² |
| Sample holder | Back mounted |
| **Sputter parameters** | |
| Sputtering beam | $Cs^+$ |
| Energy | 0.35 keV |
| Crater size | (500 µm)² |
| Sputtering time | 6s + 1s pause |
| **Mass calibration list** | |
| **Ion** | **Mass (amu)** |
| $C^-$ | 12.000549 |
| $CH^-$ | 13.008374 |
| $CH_2^-$ | 14.016199 |
| $OH^-$ | 17.003288 |
| $C_2N_2Au^-$ | 248.973249 |
| $Au_3^-$ | 590.900205 |

# 3. Results and discussion

## 3.1. AuNPs characterizations

As mentioned earlier, the mean size of the nanoparticles and their metal concentration were determined last year, for the Master 1 research project. TEM measurements showed an average AuNP diameter of 5,01 nm, with a standard deviation of 2,59 nm. The concentration of unconjucated gold was measured with AAS and was 1,074 mg/mL.

The ToF-SIMS analyses performed on the allylamine-coated AuNPs aim to identify the characteristic fragments originating from the nanoparticles. The normalized negative polarity mass spectrum is given in Figure 15 and was obtained using the analysis parameters described

in section 2.7 (sample 1). The characteristic peaks are enlarged in b). Some peaks can be attributed to different fragments composed of several gold atoms, originating from the metallic core of AuNPs. Fragments corresponding to gold bound to small polymer fragments are also present. These results indicate that the PPAA shell present on the nanoparticles does not completely shield the gold signal. Peaks related to the PPAA shell itself are not shown here. These are not of great interest from the point of view of the final application since this signal can easily be confused with that of any organic system. In fact, these are easily confused in the global organic signal when probing complex systems.

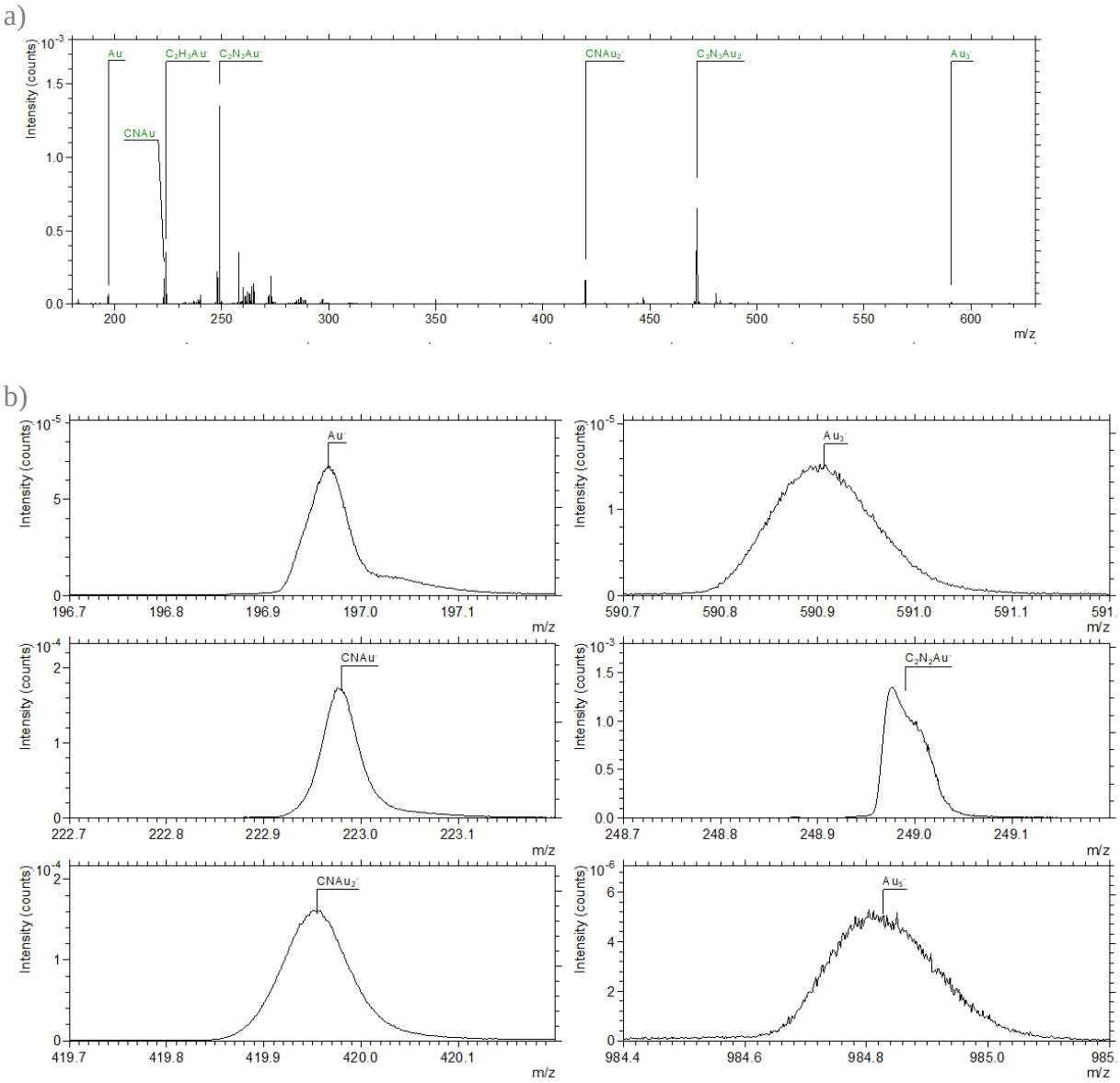


*Figure 15 : a) Mass spectrum obtained for the analysis of the AuNPs unconjugated to antibodies and b) characteristic peaks of gold fragments obtained.*

## 3.2. Bioconjugate characterizations

After carrying out the steps required for bioconjugation between AuNPs and antibodies, an AAS measurement was carried out to assess the new gold concentration. This was 276 ppm, or 0,276 mg/mL. If we compare this with the data before bioconjugation (1,074 µg/µL), we can see that the gold concentration is only a quarter of what it was before.

Pierce measurements were used to determine the protein concentration of the bioconjugate. The samples underwent two passes in the spectrophotometer :

- A first time before the addition of the Pierce reagent in order to make a blank measurement.
- A second time after the addition of the Pierce reagent.

The measurements were carried out in triplicate. The contribution of nanoparticles to the absorbance signal was considered by measuring their Pierce response in wells containing only unbound AuNPs. The Pierce assay showed a coloration of the wells and an increase in absorbance after adding the reagent, which is a first indicator that bioconjugation is working properly. Indeed, if proteins are still present in the bioconjugate, they are typically proteins conjugated to AuNPs, since unbound proteins must have been eliminated during the centrifugal diafiltration step. The antibody concentration obtained was 0.134 µg/µL. Calibration was carried out using Novex anti-mouse polyclonal antibodies used for bioconjugation. The results also show that bioconjugation resulted in a percentage of antibodies in the wells of 53,9%. According to the LARN protocol, a percentage greater than 20% indicates successful bioconjugation.

As for the stability of the ACAuNPs in triton, it was assessed after various incubation times. The UV-vis spectra are shown in Figure 16. This figure represents the normalized absorbance measured for ACAuNPs both with and without triton. The stability was evaluated every 15 minutes, up to one hour, which was the incubation time of the bioconjugated antibodies in triton for the staining experiments. The graphs demonstrate that the plasmon, located around 550 nm, remains stable upon the addition of triton to the solution, thus confirming the stability of the ACAuNPs in this detergent.

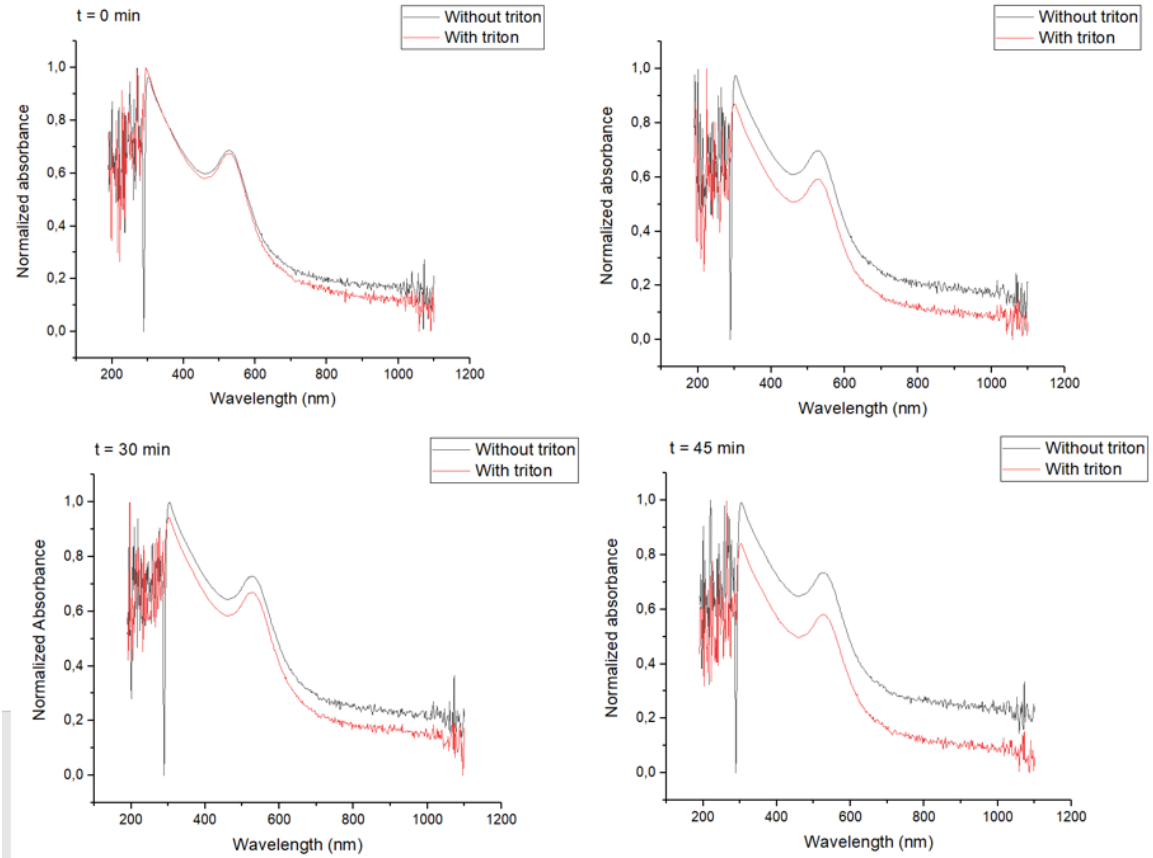

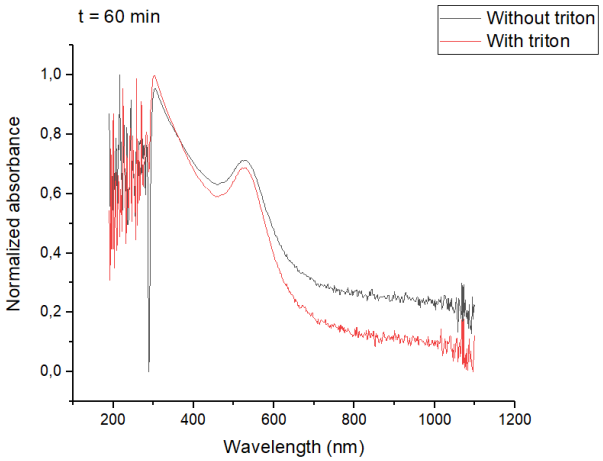


*Figure 16 :UV-visible spectra obtained by comparing the normalized absorbance of a solution of the bioconjugated antibodies with and without triton. The absorbance was measured at different incubation times ranging from 0 minutes to 60 minutes, wich represented the maximum incubation time for the staining experiments.*

## 3.3. Development of the labelling protocol

### a) Recognition between primary and secondary antibodies : ELISA assay

The ELISA assay was performed in order to verify the ability of the bioconjugated antibodies to specifically recognize and bound to their target. Two control measurements were done. The negative control corresponds to the case without the bioconjugated antibodies, in order to check the non-specific recognition of the biotinylated antibody with the anti-involucrine. A positive control was also realized, using the unconjugated antibodies, to check that they were able to recognize their target prior to bioconjugation. The bioconjugate recognition was then evaluated in duplicate using 3 different dilution factors (1:10, 1:50, 1:100). The microwell plate is shown in Figure 17, with the repartition of the sample and the absorbance measured. It can be concluded that the bioconjugated antibodies are able to detect their target, as well as the unconjugated antibodies. The negative control shows that there is no unwanted recognition.

| | A | B | C | D | E | F | G | H |
|---|---|---|---|---|---|---|---|---|
| 1 | Blank<br>Abs : 0,000 | CTL –<br>Abs : -0,038 | 1:10<br>Abs : 1,560 | 1:10<br>Abs : 1,640 | 1:50<br>Abs : 1,647 | 1:50<br>Abs : 1,594 | 1:100<br>Abs : 1,676 | 1:100<br>Abs : 1,664 |
| 2 | CTL +<br>Abs : 1,605 | | | | | | | |

*Figure 17: Plan of the ELISA multi-well plate, with the samples analysed and the measured absorbance.*

### b) Ability of the primary antibody to recognize its target : immunofluorescence staining

A set of staining experiments on RHE were performed on Superfrost+ slides in order to be analysed with a fluorescence microscope. As mentioned, several conditions were tested to verify the link between several antibodies (see Table 1). Figure 18 presents the staining of the primary antibody with a green fluorescent probe, as well as the control condition obtained by omitting the staining with anti-involucrine antibody. The control analysis a) shows almost no signal intensity when the anti-involucrine is not present, which confirms that the signal intensity in b) is not due to non-specific recognition of the fluorescent antibody. Blue spots correspond

to DAPI staining of the nucleus of keratinocytes. The staining with anti-involucrine is thus located in the SC, as expected.

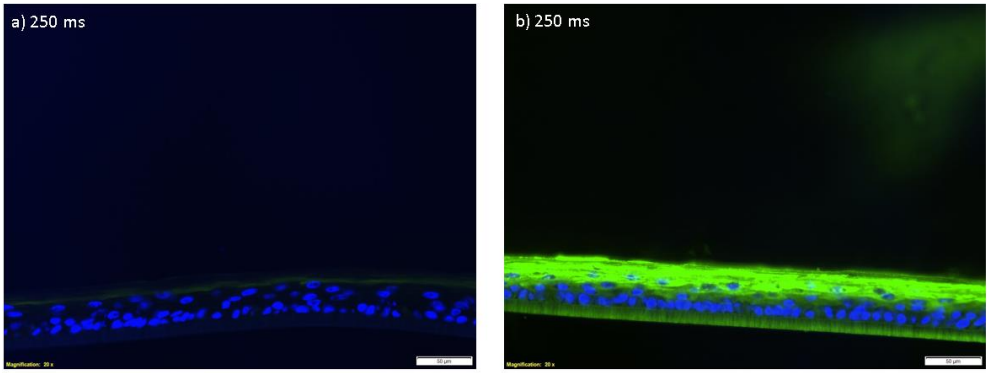


*Figure 18 : Fluorescence images obtained on a) a RHE stained without primary antibody anti-involucrine but with fluorescent secondary antibody and b) RHE stained with primary anti-body and secondary antibody. Exposition time was 250 ms*

Figure 19 presents the staining with ACAuNPs of different dilution factors and the control. The ACAuNPs were targeted by an antibody carrying a fluorescent probe. Control contains no ACAuNPs and the absence of signal intensity demonstrates that the signal present in b), c) and d) is not originating from non-specific recognition of the fluorescent antibody. The intensity of fluorescence on the sections stained with ACAuNPs increases with its concentration. Indeed, the figure shows that for a lower concentration, the exposition time must be bigger in order to have the same order of signal intensity. This shows that the bioconjugate is able to mark a protein in the RHE. However, the signal is diffuse and seem non totally specific. The stains present on the images correspond to aggregates of ACAuNPs that are not linked to a protein on the RHE.

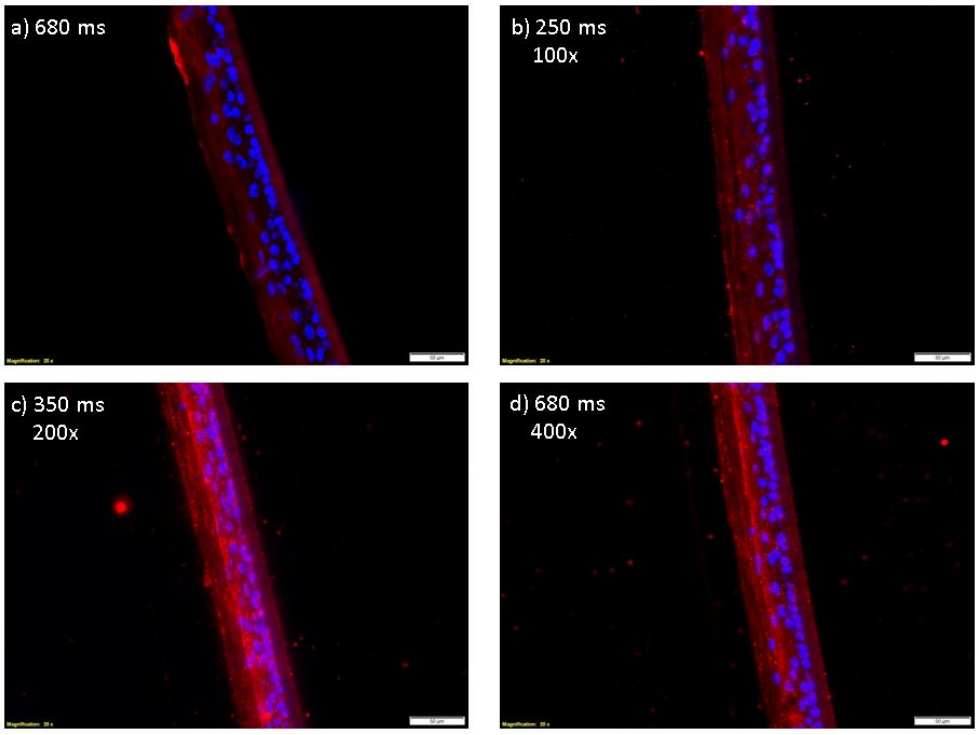


*Figure 19:Fluorescence images obtained for a) control RHE without ACAuNPs and exposition time of 680 ms, b) ACAuNPs diluted 100x and exposition time of 250 ms, c) ACAuNPs diluted 200x and exposition time 350 ms, d) ACAuNPs diluted 400x and exposition time 680 ms.*

c) Analysis with ToF-SIMS of the RHE without labelling

The RHE cross sections were cut with a microtome and were lyophilized overnight on Superfrost+ substrates. The analyses with ToF-SIMS were carried out using the parameters described above (Section 2.7, sample 2) with the purpose of obtaining an overview of the characteristic peaks recognizable on a biological sample of this type. It helped to reveal the molecular components of the RHE, providing crucial information about the orientation of the RHE on the images obtained. Indeed, fragments of polycarbonate and free fatty acids are presents in the spectra and the images corresponding to these elements make it possible to determine where the polycarbonate and the SC are. This is important in order to have a reference to compare with the position of the gold signal in the stained RHE.

Figure 20 shows images of characteristic fragments of the RHE. The polycarbonate is visible, and is the support of the RHE. Cholesterol, coming from the cholesterol sulfate, is also present, as well as free fatty acids in the SC. The RGB overlay corresponds to the several signals reunited in one image.

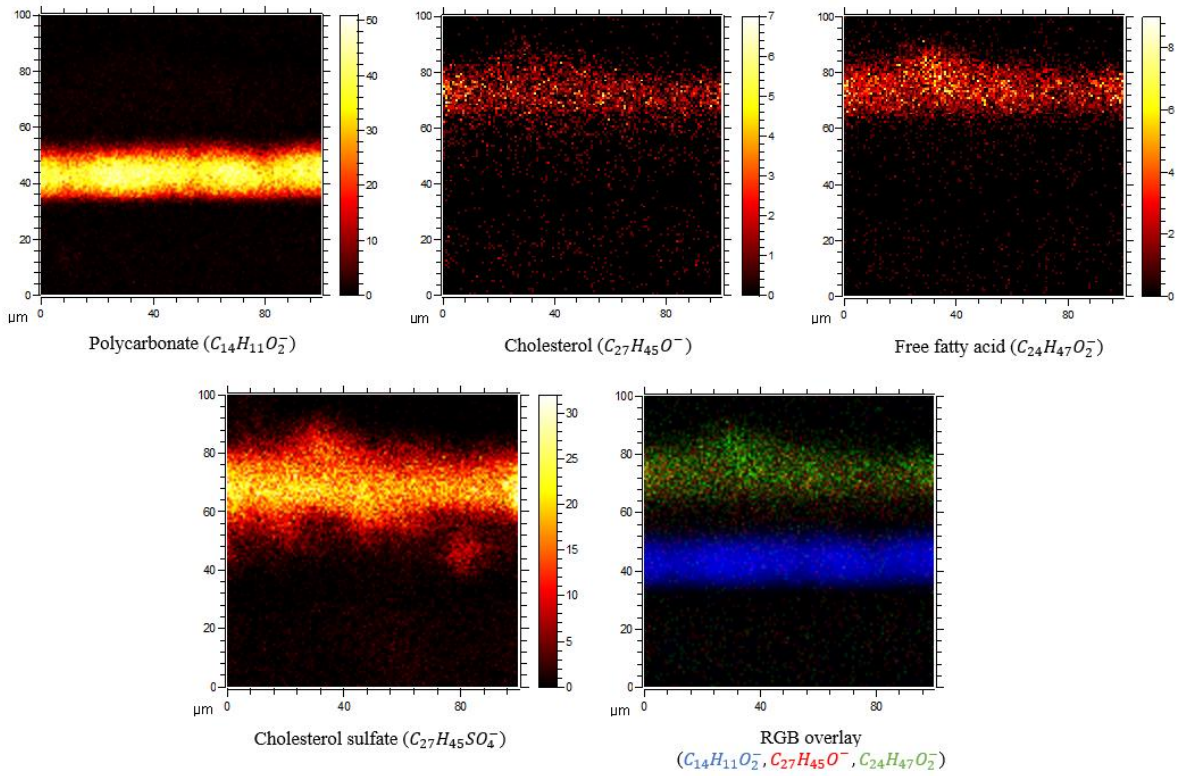


*Figure 20 : Images obtained during ToF-SIMS analyses. The polycarbonate, cholesterol, cholesterol sulfate and free fatty acid are visible on the images. The RGB overlay is also given and shows the orientation of the RHE : polycarbonate below and free fatty acid above.*

The complete peak list established based on [3,5] is also given in Table 3.

| Ion | Mass (amu) |
|---|---|
| **Cholesterol sulfate** | |
| $C_{27}H_{45}SO_4^-$ | 465.3085 |
| $C_{27}H_{46}SO_4^-$ | 466.3141 |
| $C_{27}H_{47}SO_4^-$ | 467.3148 |
| $C_{27}H_{48}SO_4^-$ | 468.3192 |

| | |
|---|---|
| $C_{27}H_{43}SO_4^-$ | 463.2991 |
| $C_{27}H_{44}SO_4^-$ | 464.2988 |
| **Cholesterol** | |
| $C_{27}H_{45}O^-$ | 385.3493 |
| $C_{27}H_{46}O^-$ | 386.3492 |
| $C_{27}H_{43}O^-$ | 383.3434 |
| $C_{27}H_{44}O^-$ | 384.3416 |
| **Polycarbonate** | |
| $C_{14}H_{11}O_2^-$ | 211.0471 |
| $C_{14}H_{12}O_2^-$ | 22.0519 |
| $C_{14}H_{10}O_2^-$ | 210.0346 |
| $C_{14}H_9O_2^-$ | 209.0286 |
| $C_{15}H_{15}O_2^-$ | 227.0832 |
| **Free fatty acids** | |
| $C_{24}H_{47}O_2^-$ | 367.3539 |
| $C_{24}H_{48}O_2^-$ | 368.3512 |
| $C_{24}H_{46}O_2^-$ | 366.3470 |
| $C_{24}H_{45}O_2^-$ | 365.3322 |
| $C_{26}H_{51}O_2^-$ | 395.3812 |
| $C_{26}H_{52}O_2^-$ | 396.3805 |
| $C_{26}H_{50}O_2^-$ | 394.3678 |
| $C_{26}H_{49}O_2^-$ | 393.3669 |

*Table 3 : Complete peaklist obtained when analysing a RHE with ToF-SIMS in negative polarity.*

### d) Cesium sputtering beam with ToF-SIMS for the labelled RHE

This set of results concerns the labelled RHE supported by silane-coated silicon wafers. The reasons for the choice of Si substrate are explained in subsection 3.3.f). The analyses were carried out using the parameters from section 2.7 (sample 4). The present section focuses on the use of the sputtering beam and its role in the work. Indeed, the first images taken in static SIMS showed no signal from gold. This result was anticipated and explained by the influence of BSA, covering the surface of the cross section itself. This resulted in the absence of the gold signal. In addition, Cs was chosen because of its ability to enhance negative ionization, which is interesting in this case as the analyses were performed in negative polarity.

The profile obtained for this acquisition is represented in Figure 21. The increase of the gold signal is visible as soon as the sputtering starts. Three peaks originating from AuNPs were unambiguously identifiable in the spectra and will therefore be the ones used to represent the AuNP signal. It is also shown that the signal of the free fatty acid decreases immediately. This is explained by the ability of the Cs sputtering beam to break large fragments into small fragments, causing a loss of its signal. Two regions of interest were defined, to separate the surface from the bulk. The ROI1 represents the first measurement, before any sputtering. The spectra coming from this portion are useful for visualizing the distribution of the polycarbonate and free fatty acids. These two elements are essential to understand where the SC is and therefore where it should be marked with the ACAuNPs. When sputtering begins, these fragments disappear but the gold signal becomes visible. The ROI2 represents the bulk, thus where the gold signal is visible. It was shield without sputtering due to the experimental steps of the labelling. Indeed, it requires several baths and the ACAuNPs are buried under BSA and other biological components.

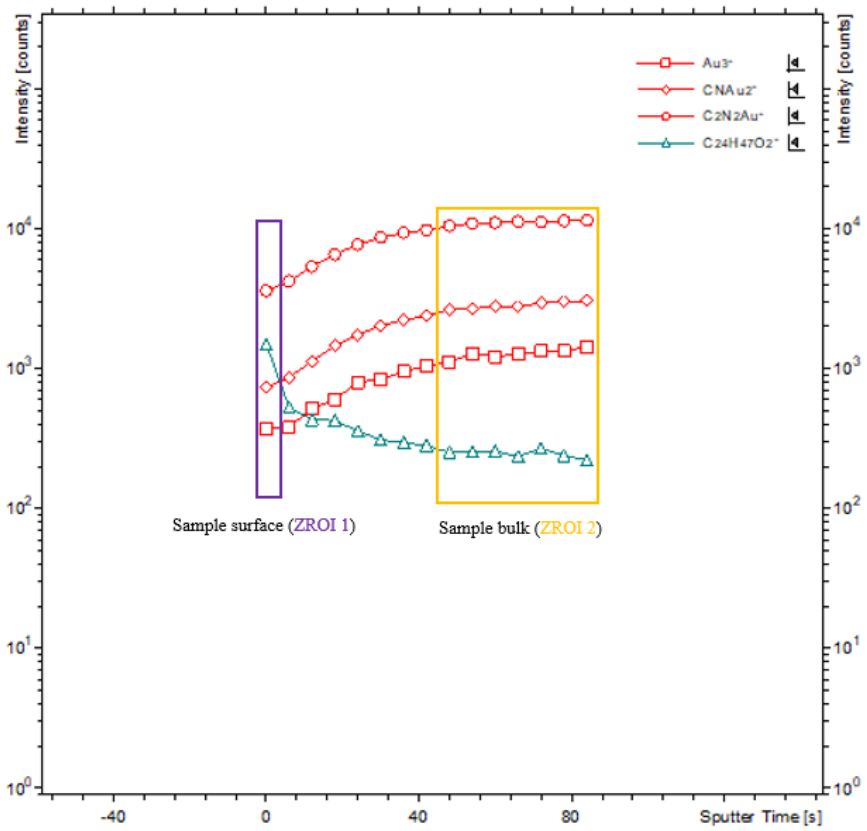


*Figure 21: Profile obtained after the sputtering of the surface of a RHE. Gold signal increases after sputtering, the ACAuNPs being buring under BSA. Two regions of interest are defined in order to make a difference between the sample surface and the bulk.*

Figure 22 shows the comparison images of the $C_2N_2Au^-$ signal induced from the surface of the sample and from the bulk, after sputtering. It should be noted that the behavior is similar for $Au_3^-$ and $CNAu_2^-$. It is observed that before sputtering, the gold signal is not present, only noise is visible. In the bulk, however (i.e. after sputtering), the gold signal is visible. The figure also shows the signal coming from the polycarbonate and free fatty acids.

When looking at the individual peaks in the mass spectrum, the same conclusions can be drawn. Figure 23 shows the peaks of the gold signal on the surface and in the bulk. A control analysis was also performed using the unconjugated antibodies, to ensure that the peaks that were attributed to AuNPs are indeed gold and not an organic fragment of the same mass. The figure shows that the signal is absent when using unbound antibodies, confirming that the signal is indeed from gold.

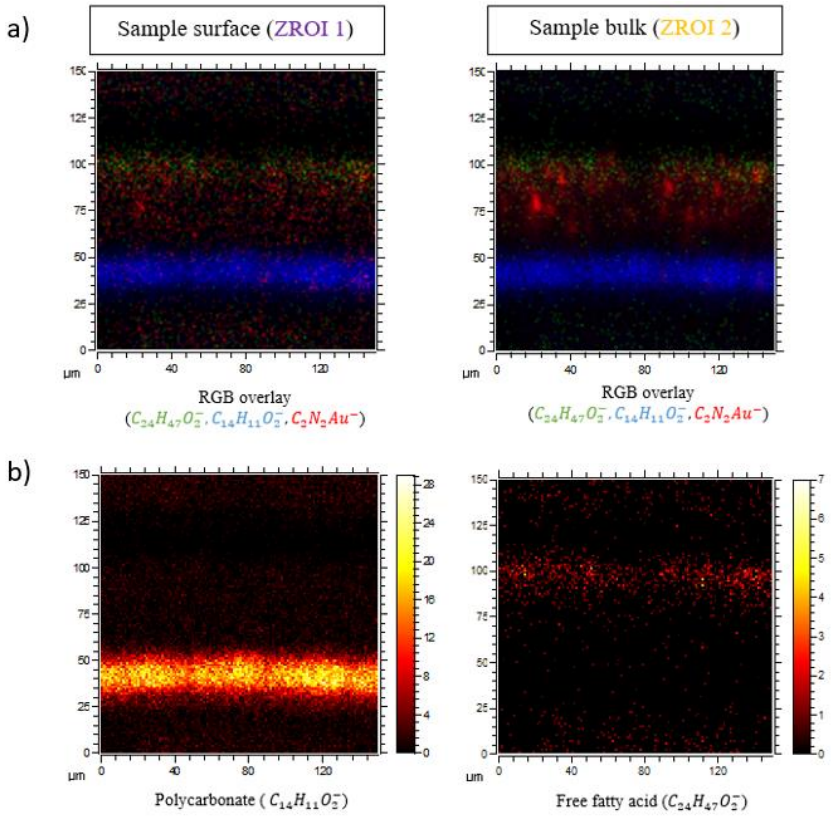


*Figure 22: Figure a) represents the gold signal on the surface of the sample and in the bulk after sputtering. Figure b) represents the polycarbonate and free fatty acid of the sample.*

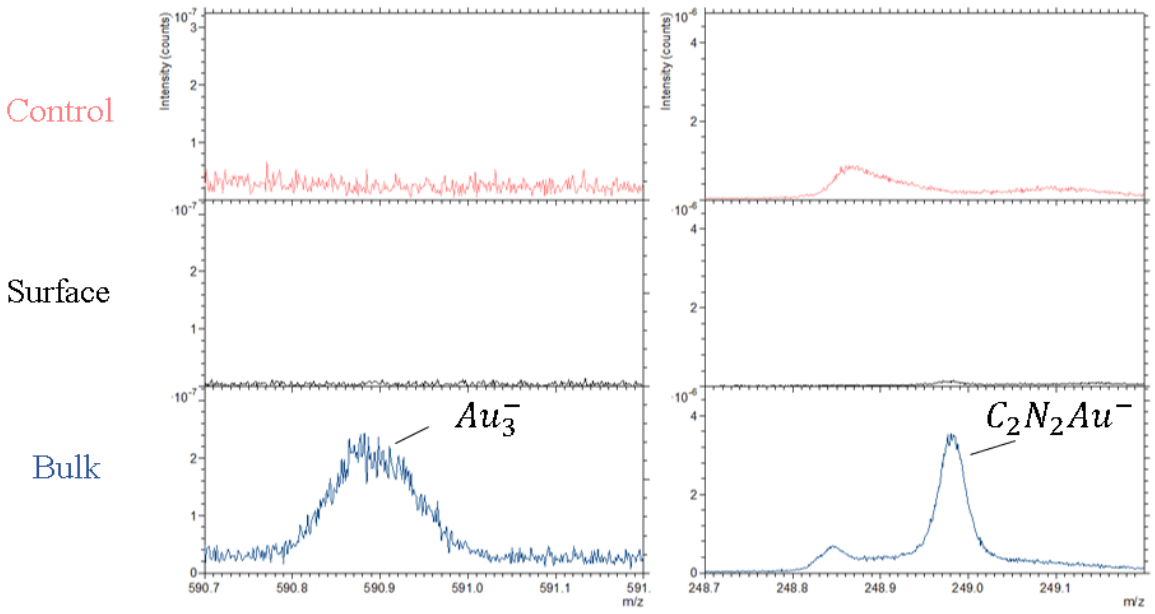

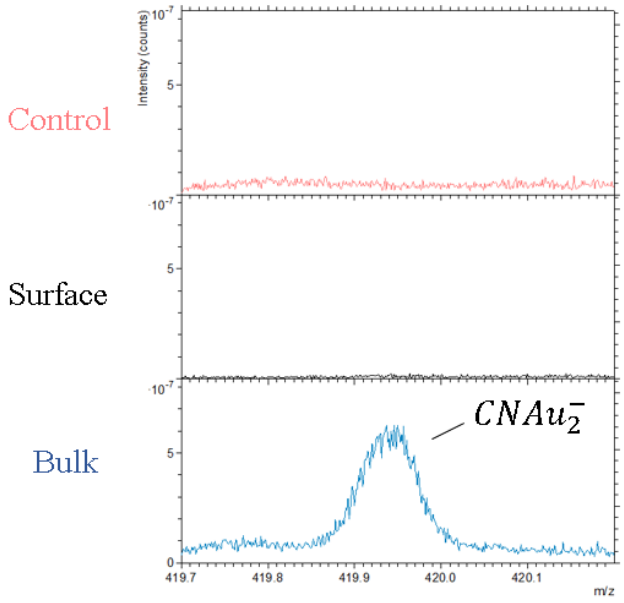


*Figure 23 : Peaks attributed to gold fragments and gold linked to organic compound. The intensity is almost zero in the control analysis and on the surface of the sample, but intensity increase when probing the bulk after sputtering.*

### e) Specificity of the marking

This experiment aims at assessing if the gold signal is related to the recognition of the target by the ACAuNPs, or if it arises from a nonspecific deposition on the RHE. In order to investigate this, an additional marking was performed, using the configuration performed without incubation of the primary antibody.

The results are shown in Figure 24.The intensity of the peaks related to the AuNPs is higher when the target of the bound antibody is present. In the case of the labelling without the primary antibody, a signal from gold is still visible, but this is due to nonspecific deposition. The fact that the intensity is lower shows that the ACAuNPs were able to reach their target, otherwise the signal would be in the same range as without the primary antibody.

Figure 25 gives a visual representation of the spatial distribution of the different fragments. The signal of $C_2N_2Au^-$ seems more intense in the SC region in the case of the primary antibody present in the marking (b). Indeed, on image a), gold signal seems to be present under the polycarbonate and above the stratum corneum (free fatty acids are not represented here due to their poor signal intensity in these specific experiments). However, this image rather shows that the marking with the ACAuNPs is not completely specific and should be optimized. Indeed, the target of the antibodies is the involucrine, which is a protein of the stratum corneum. There should be a colocalization of the gold and the free fatty acid signals. As shown in figure XX b), even though the gold signal is located in a defined area compared to a), it seems to go beyond the SC limits. An explanation for this phenomenon could be that the blocking step in the labelling protocol is not fully completed and that increasing the BSA concentration could avoid the non-specific binding in the RHE.

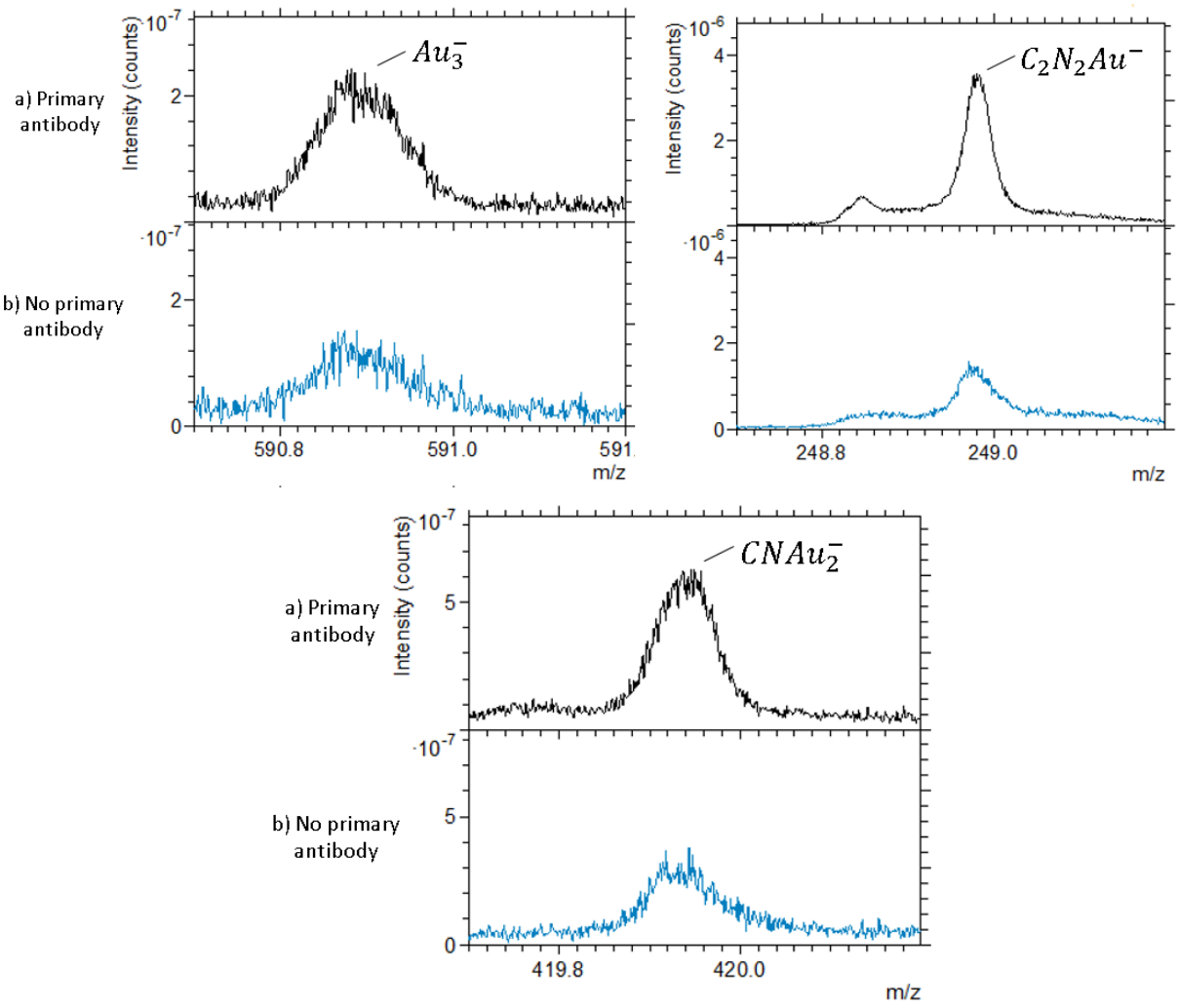


*Figure 24: Signal intensity differences between the case where the primary antibody is present or not. These images aim to show the specificity of the labelling with the ACAuNPs.*

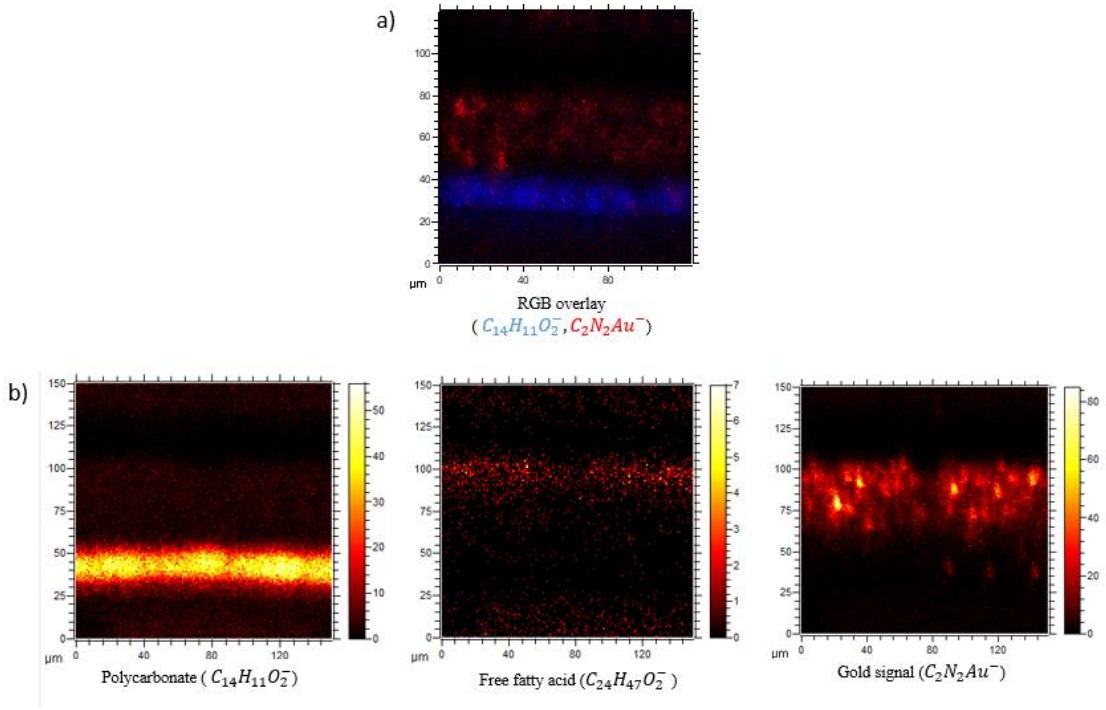

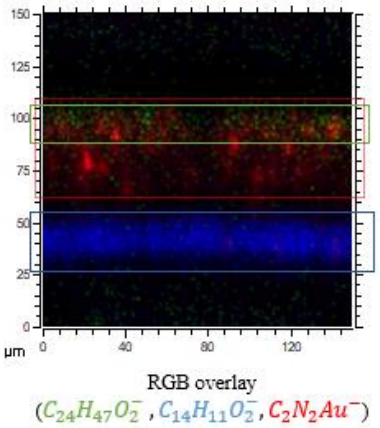


*Figure 25 : Spatial distribution of the elements when a) primary antibody is not present and when b) primary antibody is present. Gold signal seems more localised in b), but not perfectly as it is not colocalised with the free fatty acid signal. Figure b) represents the separated signals of the polycarbonate, the free fatty acids and gold as well.*

### f) Influence of the substrate

This last subsection aims to compare the results obtained with the two different substrates that were used during this work. Superfrost+ slides were first used for the labelling of the RHE in accordance with the standard IHC protocol this work is based on. This substrate is typically used for RHE staining, because its coating enhances the adhesion of the tissue and limits the loss during the staining steps. However, these slides are thicker and larger than the silicon slices that are routinely used for ToF-SIMS characterization of RHE cross sections in the laboratory. The experimenter must use the top-mounted sample holder and be extremely careful when using it, as it has no security regarding the position in height in the ToF-SIMS. This type of substrate is also non-conductive. Moreover, due to the size of these substrates, only two conditions can be observed at the same time, which limits the number of samples able to be characterized over a single day of acquisitions. The use of silicon slices is thus an alternative to this. They offer better charge compensation and can be coated with silane to improve RHE adhesion. With this kind of substrate, it is possible to use the back-mounted sample holder, which has an additional security and to test up to 9 or 10 different staining at the same time. Both substrates give good results with ToF-SIMS but silicon substrates give better mass resolution. Figure 26 presents a comparison of several peaks extracted from spectra obtained from RHE cross sections mounted either on Si slices or microscope slides. Furthermore, while charge compensation can be achieved with both substrates, silicon slices are more conducive to it due to their conductive nature, unlike Superfrost+ slides which are insulating. These several reasons support the choice of silane-coated substrates as the preferred substrate.

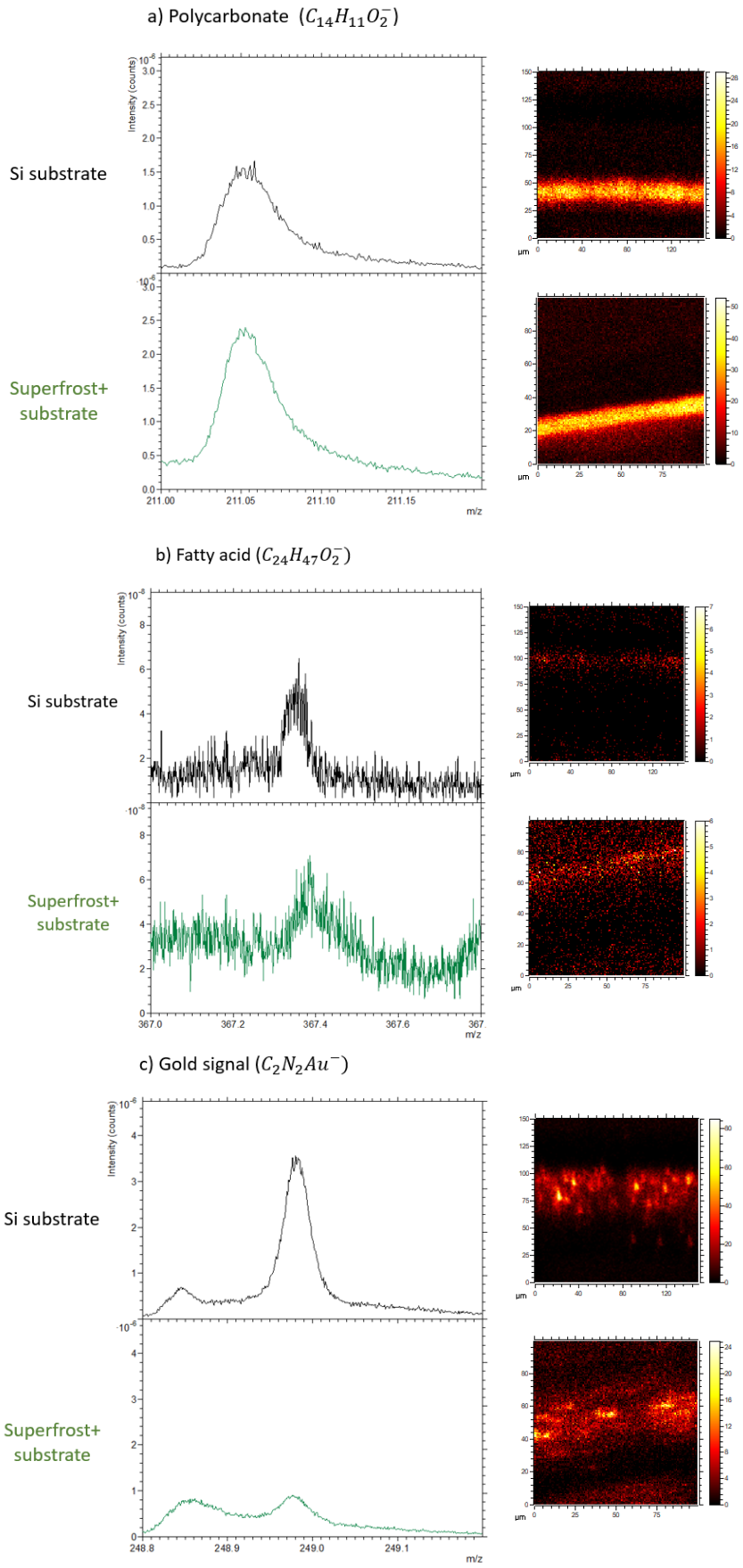


*Figure 26:Peaks and images comparison of the polycarbonate, free fatty acid and the $C_2N_2Au^-$on the Si substrate and the superfrost+ substrate.*

# 4. Conclusion and perspectives

During this thesis, AuNPs were synthetized via magnetron sputtering, yielding gold NPs encapsulated by a PPAA coating. This PPAA shell gives the possibility to link the AuNPs to antibodies. This was achieved according to a patent developed by the LARN. The obtained bioconjugate was characterized by AAS, Pierce assay and UV-vis spectroscopy. The general goal of this work is to specifically target a protein in a reconstructed human epidermis and tag it with a metallic NP, in order to characterize its distribution in ToF-SIMS, and therefore map the distribution of the investigated protein. The recognition between the target and the bioconjugate was checked thanks to an ELISA assay.

RHE were produced in the LabCeTi and were analysed with ToF-SIMS to obtain information about the organic signal visible. Polycarbonate and free fatty acids are easily recognizable and their signal was used to determine the orientation of the RHE on the images and precisely locate the SC region. Several staining conditions were tested. Notably, the influence of the concentration in AuNPs and the type of substrate were investigated. In parallel, immunofluorescence assays showed that both the primary and AuNP-conjugated antibodies were able to detect their target.

ToF-SIMS results showed that dynamic SIMS was necessary to observe a gold signal. Cesium sputtering was used to remove surface pollution, mostly due to BSA. This etching step reveals the gold signal and the images show that the signal seems located around the SC. However, the colocalization between the free fatty acids and gold signals was not as expected, revealing a non-specific contribution in the labelling. A difference was also observed when using glass substrate or Si substrate, revealing that Si slices are more suitable for analysis of RHE with ToF-SIMS. This is explained by the conductive nature of the Si, that improves charge compensation.

This work led to the successful design of a staining protocol allowing to label specific proteins with a metallic NP probe. In parallel, it allowed to determine the adequate ToF-SIMS analysis conditions required to characterize such systems. Although the quality of the stainings realized in the context of this work proved to be partially impaired by a non-specific labelling, it helped pave the way for further investigations on the topic. Most notably, since the end of this project, more recent experiments based on these findings allowed to obtain a specific labelling of involucrine by increasing the concentration of BSA during blocking steps.

# Bibliography


[1] R. N. S. Sodhi, “Time-of-flight secondary ion mass spectrometry (TOF-SIMS): - Versatility in chemical and imaging surface analysis,” Analyst, vol. 129, no. 6, pp. 483–487, 2004.

[2] H. Mei, T. S. Laws, T. Terlier, R. Verduzco and G. E. Stein, “Characterization of polymeric surfaces and interfaces using time-of-flight secondary ion mass spectrometry,” Journal of Polymer Science. John Wiley and Sons Inc, 2021.

[3] P. Sjövall, L. Skedung, S. Gregoire, O. Biganska, F. Clément and G. S. Luengo, “Imaging the distribution of skin lipids and topically applied compounds in human skin using mass spectrometry,” Sci. Rep., vol. 8, no. 1, p. 16683, Dec. 2018.

[4] S. Fearn, “Characterisation of biological material with ToF-SIMS: A review,” Materials Science and Technology (United Kingdom), vol. 31, no. 2. Maney Publishing, pp. 148–161, 01-Jan-2015.

[5] Delvaux, X., Noël, C., Poumay, Y., & Houssiau, L. (2023). Probing the human epidermis by combining ToF-SIMS and multivariate analysis. Biointerphases, 18(1), 011002. https://doi.org/10.1116/6.0002289

[6] Poumay, Y., & Coquette, A. (2007). Modelling the human epidermis in vitro : tools for basic and applied research. Archives of Dermatological Research, 298(8), 361-369. https://doi.org/10.1007/s00403-006-0709-6

[7] D. Bonifazi, V. Corvaglia, R. Marega and S. Lucas, “Method for functionalizing nanoparticles,” 2018.

[8] S. Li et al., “Antibody-functionalized gold nanoparticles as tumor-Targeting radiosensitizers for proton therapy,” Nanomedicine, vol. 14, no. 3, pp. 317–333, Feb. 2019.

[9] Vickerman, J. C., & Briggs, D. (2013). ToF-SIMS : Materials Analysis by Mass Spectrometry. IM Publications.

[10] SPHYM226, “Techniques de caractérisation des surfaces et interfaces”, Colaux, J., Houssiau, L., 2022-2023, Cours Université de Namur, Master 2 Physique à finalité approfondie.

[11] Brison, J., Mine, N., Wehbe, N., Gillon, X., Tabarrant, T., Sporken, R., & Houssiau, L. (2012). Molecular depth profiling of model biological films using low energy monoatomic ions. International Journal of Mass Spectrometry, 321-322, 1-7. https://doi.org/10.1016/j.ijms.2012.04.001

[12] Brison, J., Mine, N., Poisseroux, S., Douhard, B., Vitchev, R., & Houssiau, L. (2007). Measurement and modeling of work function changes during low energy cesium sputtering. Surface Science, 601(6), 1467-1472. https://doi.org/10.1016/j.susc.2006.12.078

[13] Houssiau, L., & Mine, N. (2010). Molecular depth profiling of polymers with very low energy reactive ions. Surface and Interface Analysis, 42(8), 1402-1408. https://doi.org/10.1002/sia.3159

[14] Khan, I., Saeed, K., & Khan, I. A. (2017). Nanoparticles : Properties, applications and toxicities. Arabian Journal of Chemistry, 12(7), 908-931. https://doi.org/10.1016/j.arabjc.2017.05.011

[15] Mittal, A., Chisti, Y., & Banerjee, U. C. (2013). Synthesis of metallic nanoparticles using plant extracts. Biotechnology Advances, 31(2), 346 356. https://doi.org/10.1016/j.biotechadv.2013.01.003

[16] Huang, J., Li, Q., Sun, D., Lu, Y., Su, Y., Yang, X., Wang, H., Wang, Y., Shao, W., He, N., Hong, J., & Chen, C. (2007). Biosynthesis of silver and gold nanoparticles by novel sundriedCinnamomum camphoraleaf. Nanotechnology, 18(10), 105104. https://doi.org/10.1088/0957-4484/18/10/105104

[17] Yeh, Y., Creran, B., & Rotello, V. M. (2012). Gold nanoparticles : preparation, properties, and applications in bionanotechnology. Nanoscale, 4(6), 1871-1880. https://doi.org/10.1039/c1nr11188d

[18] Zhao, P., Li, N., & Astruc, D. (2013). State of the art in gold nanoparticle synthesis. Coordination Chemistry Reviews, 257(3-4), 638-665. https://doi.org/10.1016/j.ccr.2012.09.002

[19] Mehran, Q., Fazal, M., Bushroa, A. R., & Rubaiee, S. (2018). A Critical Review on Physical Vapor Deposition Coatings Applied on Different Engine Components. Critical Reviews in Solid State and Materials Sciences, 43(2), 158-175. https://doi.org/10.1080/10408436.2017.1320648

[20] Geyao, L., Yang, D. J., Wanglin, C., & Chengyong, W. (2020). Development and application of physical vapor deposited coatings for medical devices : A review. Procedia CIRP, 89, 250-262. https://doi.org/10.1016/j.procir.2020.05.149

[21] Stoner, J. (2023, 1 février). What is Magnetron Sputtering and How Does it Work | Korvus Technology. Korvus Technology. https://korvustech.com/magnetron-sputtering/

[22] Behera, A., Aich, S., & Theivasanthi, T. (2022). Magnetron sputtering for development of nanostructured materials. Dans Elsevier eBooks (p. 177-199). https://doi.org/10.1016/b978-0-12-820558-7.00002-9

[23] N. Moreau et al., "PVD synthesis and transfer into water-based solutions of functionalized gold nanoparticles," in Plasma Processes and Polymers, 2009, vol. 6, no. SUPPL. 1.

[24] Tsai, W., & Wu, A. H. (2018). Aligning physics and physiology : Engineering antibodies for radionuclide delivery. Journal of Labelled Compounds and Radiopharmaceuticals, 61(9), 693-714. https://doi.org/10.1002/jlcr.3622

[25] D. Bonifazi, V. Corvaglia, R. Marega, and S. Lucas, "Method for functionalizing nanoparticles," 2018.

[26] S. Li et al., "Antibody-functionalized gold nanoparticles as tumor-Targeting radiosensitizers for proton therapy," Nanomedicine, vol. 14, no. 3, pp. 317–333, Feb. 2019.

[27] M. Akhyar Farrukh, Ed., Atomic Absorption Spectroscopy. InTech, 2012.

[28] Antharavally, B. S., Mallia, K. A., Rangaraj, P., Haney, P. M., & Bell, P. M. (2009). Quantitation of proteins using a dye–metal-based colorimetric protein assay. Analytical Biochemistry, 385(2), 342-345. https://doi.org/10.1016/j.ab.2008.11.024

[29] De La Rica, R., & Stevens, M. M. (2012). Plasmonic ELISA for the ultrasensitive detection of disease biomarkers with the naked eye. Nature Nanotechnology, 7(12), 821-824. https://doi.org/10.1038/nnano.2012.186

[30] Lakshmipriya, T., Gopinath, S. C. B., & Tang, T. (2016). Biotin-Streptavidin Competition Mediates Sensitive Detection of Biomolecules in Enzyme Linked Immunosorbent Assay. PLOS ONE, 11(3), e0151153. https://doi.org/10.1371/journal.pone.0151153

[31] Edinburgh Instruments Ltd. (2023, 18 avril). UV Vis Spectroscopy | Spectrometer | Spectroscopy Applications. Edinburgh Instruments. https://www.edinst.com/techniques/uv-vis-spectroscopy/?fbclid=IwAR0VxJ52702YqDGBzG6Vxyh10xcAJX8PhACcCo5Gl6TCHsg25_bV4yXZa_w

[32] Cytodiagnostics Inc. (s. d.). Introduction to Gold Nanoparticle Characterization. https://www.cytodiagnostics.com/pages/introduction-to-gold-nanoparticle-characterization

[33] Poumay, Y., Dupont, F., Marcoux, S., Leclercq-Smekens, M., Hérin, M., & Coquette, A. (2004). A simple reconstructed human epidermis : preparation of the culture model and utilization in in vitro studies. Archives of Dermatological Research, 296(5), 203-211. https://doi.org/10.1007/s00403-004-0507-y

[34] Faway, E., Cambier, L., Mignon, B., Poumay, Y., & De Rouvroit, C. L. (2016). Modeling dermatophytosis in reconstructed human epidermis : A new tool to study infection mechanisms and to test antifungal agents. Medical Mycology. https://doi.org/10.1093/mmy/myw111

[35] OCT Compound 118ml. (s. d.). https://www.agarscientific.com/oct-compound, consulted on 30 march 2023.

[36] Epredia&trade ; ; SuperFrost Plus&trade ; Adhesion slides - Glass Microscope Slides and Coverslips Beakers, Bottles, Cylinders and Glassware. (s. d.). https://www.fishersci.be/shop/products/superfrost-plus-adhesion-slides-9/p-7112218#?keyword , consulted on 30 march 2023.

[37] Immunohistochemistry fixation protocol | Abcam. (2023, 26 avril). https://www.abcam.com/protocols/ihc-fixation-protocol, consulted on 3rd may 2023.

**Error! Use the Home tab to apply Appel note de bas de p. to the text that you want to appear here.**